

~~A regional analysis of paraglacial landslide~~ Landslide activation during deglaciation in a fjord-dominated landscape: observations from southern ~~coastal~~ Alaska (1984-2022)

Jane Walden^{1,2}, Mylène Jacquemart^{1,2}, Bretwood Higman³, Romain Hugonnet^{1,2,4}, Andrea Manconi^{5,6}, and Daniel Farinotti^{1,2}

¹Laboratory of Hydraulics, Hydrology and Glaciology (VAW), Swiss Federal Institute of Technology (ETH), Zurich, Switzerland

²Swiss Federal Institute for Forest, Snow and Landscape Research (WSL), bâtiment ALPOLE, Sion, Switzerland

³Ground Truth Trekking, Seldovia, AK, USA

⁴Department of Civil and Environmental Engineering, University of Washington, Seattle, WA, USA

⁵Institute for Snow and Avalanche Research (SLF), Swiss Federal Institute of Forest, Snow and Landscape Research (WSL), Davos, Switzerland

⁶Department of Earth and Planetary Sciences, Swiss Federal Institute of Technology (ETH) Zurich, Zurich, Switzerland

Correspondence: Jane Walden (walden@vaw.baug.ethz.ch)

Abstract.

~~Glaciers worldwide are retreating rapidly due to anthropogenic climate change. One consequence of~~ A consequence of the current global glacier mass loss is the destabilization of valley walls as the support provided by the glacier ~~changes~~ evolves and eventually vanishes, a process ~~known~~ typically referred to as “debuttressing.” In this work, we ~~examine~~ examined the evolution of eight large, active ~~instabilities~~ landslides in southern coastal Alaska, a region experiencing some of the fastest glacier ~~retreat~~ worldwide. ~~At half of the sites, the glacier is still~~ mass loss worldwide. Additionally, many glaciers in this area are retreating out of glacially carved fjords, leaving landslides in contact with ~~the landslide~~, while in the other four cases, the terminus retreated past the landslide in recent decades. One site has experienced catastrophic failure; the others have not. We ~~use~~ deep water bodies that can substantially increase the reach of a catastrophic failure. We used automatic and manual feature tracking on optical imagery to derive slope movement from the 1980s to present and ~~compare~~ compared this with glacier terminus retreat and thinning, precipitation, and seismic energy. ~~We find~~, paying particular attention to landslides in contact with lake or ocean water. We found that the majority of ~~sites~~ landslides underwent a pulse of accelerated ~~landslide motion~~ (up to 17 times higher compared to the five years preceding the acceleration) motion during the studied time period ~~and that the subsequent deformation was independent of the initial activation~~. In two cases, the acceleration occurred after a particularly ~~rainy month and/or a marked increase (around two~~. In four cases, landslide movement coincided with the rapid retreat of a lake- or marine-terminating glacier past the instability. At these sites and during these accelerations, the glacier retreat rates were up to 7 times higher than ~~the 1960-2000 average~~ in glacier thinning. At two further sites, no distinct activation could be ~~detected~~ average, while the landslides reached velocities that were up to 9 times higher than their long-term average. Two sites showed no movement, though both landslides are known to be moving at velocities below the detection threshold of the methods employed here. ~~In four cases, landslide activation coincided with the rapid retreat (up to 12 times the long-term average) of a~~

~~lake-or-marine-terminating-glacier-past-the-instability~~At two other sites where the landslides are still in contact with the ice, above-average precipitation and increased glacier thinning were found to coincide with accelerated motion, though conclusive causal links could not be drawn and the effect of short-term precipitation could not be ruled out. Our results suggest that landslides adjacent to ~~lake-or-marine-terminating-glaciers~~ lakes or fjords may be especially susceptible to sudden activation, which we ~~hypothesize~~ propose is due to the ~~faster~~ particularly rapid retreat rates of water-terminating glaciers as well as mechanical and hydrological changes resulting from the replacement of ice with water at the landslide toe. ~~This work shows that glacier retreat can be associated with increasing landslide hazards in various glaciological~~ in relatively short timescales. By showing that glacier mass loss is associated with increased landslide movement across various settings in Alaska, ~~which has implications for the assessment of hazards~~ we suggest that glacier-landslide interactions in coastal settings deserve special attention and further substantiate the need for establishing broader and more systematic paraglacial hazard monitoring in a warming world.

1 Introduction

Anthropogenic climate change is causing rapid glacier thinning and retreat all over the world (IPCC, 2022). ~~This glacier~~ Glacier mass loss has a wide variety of impacts on the Earth system and human livelihoods, ~~such as diminished water resources and~~ sea level rise ~~and changes to glacier runoff being among the most consequential~~ (IPCC, 2019; Immerzeel et al., 2020). Glacier retreat ~~may also lead to the destabilization of~~, which removes support from adjacent valley walls ~~and this “debuitressing” effect (Ballantyne, 2002) may culminate in the~~ in a process termed “glacier debuitressing” (Ballantyne, 2002), may lead to the ~~destabilization or~~ failure of weakened valley slopes. ~~Given that such slopes are often in areas~~ There is limited direct risk to humans from such slow-moving slopes, since these areas are too dynamic to support human infrastructure, ~~there is limited~~ direct risk from landslides. However, ~~they catastrophic slope failure~~ can have significant downstream impacts by damming rivers ~~that might breach as outburst floods, or by erosion of landslide deposits, which can abruptly increase sediment transport or abruptly increasing sediment input into proglacial water systems~~ (Fan et al., 2020). Additionally, landslides can initiate highly mobile cascading processes which may threaten critical infrastructure (e.g., Van Wyk de Vries et al., 2022; Shugar, D.H. et al., 2021; Sharma et al., 2023).

Where catastrophic landslides enter water, such as proglacial lakes or fjords, they can generate tsunamis. ~~Landslide-tsunami cascades have received attention after several events in deglaciating regions caused destruction and loss of life~~ Albeit comparatively rare, landslide-tsunami cascades can have far-reaching and destructive impacts, as is exemplified by several cases from the last decades. In 1958, for example, a landslide near the terminus of Lituya Glacier, Alaska, impacted Lituya Bay, generating a tsunami that ran up 530 m on a nearby ridge ~~and killed two people~~ (Miller, 1960). Less than a decade later, an instability near Grewingk Glacier, Alaska, failed catastrophically into a proglacial lake and caused a tsunami with 60 m runup (Wiles and Calkin, 1992; Lemaire et al., 2023a). In 2000, a large landslide entered the Vaigat Strait in western Greenland, generating a tsunami with a 28 m runup in a town 20 km away from the source (Dahl-Jensen et al., 2004). In 2015, a large landslide in Taan Fiord, Alaska, caused a tsunami with 193 m runup (Higman et al., 2018). Two years later, in Karrat Isfjord, western Greenland, a large landslide failed catastrophically into a fjord, generating a tsunami with 90 m runup near to the failure site, and the tsunami inundated a village 32 km away with 1 to 1.5 m waves ~~(Strzelecki and Jaskólski, 2020)~~, killing four people (Strzelecki and Jaskólski, 2020). More recently, in 2023, a large landslide impacted a fjord in Dickson Fjord, eastern Greenland, causing a 200 m runup followed by a seiche which generated a seismic signal lasting for 9 days (Svennevig et al., 2024). Despite the destructive potential of these events, few ~~cases have been studied in depth, especially in relation to glacier retreat~~ studies have investigated landslide evolution near deep fjords with a specific focus on the glacier evolution.

~~There is still much~~ Much remains unknown about how glacial erosion and debuitressing ~~may precondition slopes for failure~~. Higman et al. (2018) ~~identified potential triggering factors at~~ interact with other factors to precondition or trigger slope failures. In fact, there has been some debate about whether glacier debuitressing can cause slope failure due to the viscous nature of ice at low strain rates (McColl et al., 2010; McColl and Davies, 2013; Storni et al., 2020). Others suggest that debuitressing can increase shear stress and act in combination with other processes such as rainfall to promote slope movement (Le Roux et al., 2009). At Taan Fiord, ~~such as above-average rainfall and an earthquake~~, also noting how the were identified

as potential triggering factors, though the authors note that the glacier retreated over 17 km in 50 years and thinned by 400 m from 1961–1991. In the Grewingk case, the exact cause of the failure remains unknown 1961–1991 (Higman et al., 2018). At Grewingk Lake, a specific trigger could not be identified, though it is thought that the slope was weakened by a large earthquake in 1964, a month of intense precipitation, and multiple cycles of glacier retreat (Wiles and Calkin, 1992; Lemaire et al., 2023a). Specifically, upon the formation of the proglacial lake, retreat sped up significantly due to ice loss by calving (Wiles and Calkin, 1992). Here, too, the glacier retreat is thought to have played a role in slope destabilization. Precipitation can cause groundwater fluctuations which impact landslide stability (e.g., Handwerger et al., 2019a; Iverson, 2000) and seismic shaking has been shown to weaken slopes (Keefer, 1984; Lacroix et al., 2014), resulting in varying behavior during and after earthquakes (Kohler and Puzrin, 2023). In addition, litho-structural characteristics (Kuhn et al., 2023; Stead and Wolter, 2015), rock mass properties (Wang et al., 2021; Gischig et al., 2016; Hugentobler et al., 2022), and changing lake water levels (Hendron and Patton, 2001) are among the mechanisms which drive landslide motion. All of these processes—as well as combinations of them—may be relevant to the sites studied here.

Connections between glacier and landslide changes have been documented at several sites around the world. At the Barry Arm landslide in southern Alaska, dramatic landslide acceleration was correlated with rapid glacier retreat (Dai et al., 2020). Interestingly, the kinematic response of the slope to deglaciation has changed throughout time (Schaefer et al., 2023). In a more alpine setting, the landslide at Tungnakvíslarjökull in Iceland sped up after the glacier mass loss increased, and glacier debuttressing was determined to be the main cause of slope acceleration (Lacroix et al., 2022). Studies of the Moosfluh landslide in Switzerland showed that glacier unloading and altered groundwater creates critical conditions leading landslide deformation can be related to debuttressing, with landslides reacting rapidly to glacier changes upon crossing a threshold of ice loss (Kos et al., 2016). Others found that the glacier controls the landslide velocity but has little effect on its stability (Storni et al., 2020), and Glueer et al. (2020) suggested that altered groundwater conditions may lead to enhanced slope instability (Glueer et al., 2020). Numerical models show that thermo- and hydro- mechanical stresses from repeated glacier cycles weaken rock (Grämiger et al., 2018, 2020), and most rock damage occurs upon first deglaciation (Grämiger et al., 2017). Further studies found that the glacier controls the landslide velocity but has little effect on its stability (Storni et al., 2020), and suggested that landslides react rapidly to glacier changes upon crossing a threshold of ice loss (Kos et al., 2016).

These examples indicate that ice loss, whether it be thinning or retreat, is connected to slope instability. They also demonstrate a connection between ice loss and slope stability and bring attention to a hazard that is not yet well understood. Alaska ; in particular, has is a hotspot for glacier mass loss, making up ~25 % of global glacier mass loss between 2000 and 2020 (Hugonnet et al., 2021), despite containing only around 12% of the world's glacier volume (Farinotti et al., 2019). Alaska has also come to light as a region where there exists with a precarious combination of paraglacial landslide formation landslides and rapidly retreating tidewater or lake-terminating glaciers (Schaefer et al., 2024). This (We use “paraglacial” to define non-glacial processes impacted by glaciation (Church and Ryder, 1972)). The increased awareness of this hazard spurred the creation of an Alaskan landslide inventory (Higman, 2022; Higman et al., 2023), which documents instabilities both pre- and post-failure , relict landslides, and mass movement deposits throughout the state. Alaska is also a hotspot for rapid glacier retreat, making up a quarter of global Given that the high rates of glacier mass loss between 2000 and 2020 (Hugonnet et al., 2021), despite

containing only around 12% of the world's glacier volume (Farinotti et al., 2019). Glaciers are projected to continue losing mass at high rates throughout during the 21st century (Rounce et al., 2023), which prompts the question of, it is of interest to determine how the risk posed by paraglacial landslides and potential tsunamis will change in the future.

To understand how glacier thinning and retreat control landslide activation and mobility, we take a synoptic view of eight large paraglacial landslides in southern Alaska (Sect. 2) and analyze their evolution using satellite imagery from 1984 until present, surface velocity changes from 1984–2022, and elevation changes from the mid-1900s until 2020. By doing so, we provide the first detailed regional study examining the impact of glaciers on slope stability in study comparing detailed glacier evolution—including both thinning and terminus retreat—with landslide movement in southern Alaska. Specifically, we ask whether the (re-)activation of paraglacial landslides can be explained by glacier retreat. In order to evaluate the relevance of the glacier changes, we also consider meteorological and seismic influences (Sect. 3). We combine these data to assess whether and how glacier changes can be responsible for slope destabilization (Sect. 4) and discuss these in the context of the possible physical mechanisms behind the slope instabilities (Sect. 5).

2 Study Area

Southern Alaska is heavily glaciated, hosting some of the largest glaciers in the world (Windnagel et al., 2023). It has a maritime climate due to its proximity to the ocean, it has a maritime climate, leading to high annual precipitation and in turn, extensive glacier coverage (Shulski and Wendler, 2007). Over the eight study sites (Fig. 1) and the period 1979–2022, annual precipitation ranges 1979–2022, average annual precipitation ranged from 2670 to 4030 mm while mean annual air temperatures are varied between -4 and 1°C (Hersbach et al., 2018). These 3°C (Hersbach et al., 2018). The large precipitation amounts result in a thick winter snowpack which, combined with relatively mild temperatures, make extended permafrost coverage unlikely (Figure 1; Obu et al., 2018).— less than a 1% probability of occurrence at our sites according to Obu et al. (2018) (Fig. 1).

Alaska is a very seismically active region and experiences some of the highest uplift rates worldwide (Larsen et al., 2005). Glacier mass loss since the Little Ice Age in Alaska is resulting in high isostatic rebound rates. This, in combination with the Alaska's and the location on a subduction zone, causes some of the world's highest uplift rates: result in uplift rates as high as 10 mm yr^{-1} on the Kenai Peninsula (Cohen and Freymueller, 2001) and up to 32 mm yr^{-1} in southeastern Alaska. In this area, up to 5 mm yr^{-1} of the total uplift is due tectonic forcing, 2 to 4 mm yr^{-1} comes from global glacier isostatic adjustment, as much as 13 mm yr^{-1} are due to current glacier mass loss, and the rest (ca. 10 mm yr^{-1}) are due to viscoelastic uplift southeast Alaska (Larsen et al., 2005). The collision of the Pacific and North American plates has formed several major faults throughout the state. The Castle Mountain, Border Ranges, and Fairweather faults are the most relevant for this work (Mériaux et al., 2009). Alaska is one of the most seismically active regions in the world, having has had four of the twenty largest earthquakes recorded globally since 1900 (Earthquake Hazards Program, 2019), and with an earthquake of magnitude eight or larger every 13 years since 1900 (Alaska Seismic Hazards Safety Commission, 2012). The state also sees many moderate earthquakes of magnitude 4 to 5 (magnitude 4–5): on average, 300 per year since 1900 (Alaska Seismic Hazards Safety Commission, 2012).

Study sites were selected from the *Alaska inventory of landslides and slope instabilities* (Higman, 2022; Higman et al., 2023). In line with the terminology used in the inventory, we use the terms “landslide” and “instability” interchangeably throughout this publication. The inventory contains over 780 landslides at the time of publication, and details the instability characteristics, location, date of slope failure (if available), volume, and the hazard potential to communities and infrastructure. From the complete Higman (2022) inventory, we selected a subset of eight sites in eight instabilities which are distributed throughout southern coastal Alaska that met the following criteria: Volume estimated to be greater than 10 Mio.m³, In from the Kenai Peninsula to Glacier Bay and have all been in contact with a glacier at some stage since the 1980s. The selection was relatively arbitrary, focusing on sites that stood out as worth investigating from early versions of the inventory. At four sites—Ellsworth, Portage, Geomorphic signs of recent movement after the mid-1980s. If there were several sites in a close proximity that matched these criteria, the largest and most active instability was selected. The selected sites are shown in Figure 1 and Figure 2, and are described further in the following subsections.

2.1 Ellsworth

Ellsworth Glacier is a lake-terminating glacier located on the Kenai Peninsula, around 30 km east of Seward, Alaska (Fig. 1B and Fig. 2). It is oriented to the southwest and flows from a glacier complex at over 1800 m a.s.l. to nearly sea level (10 m a.s.l.). There are a series of instabilities along the western edge of the glacier, where the glacier bends. We focus on the instability which is largest and farthest up-glacier, spanning a distance between 2.5 and 4 km from the 2021 terminus. The instability is characterized by a prominent main scarp and an active talus source area (Higman et al., 2023). Movement at the site between 2016 Columbia, and 2022 has been confirmed by Schaefer et al. (2024) using interferometric synthetic aperture radar (InSAR). The instability is located in sedimentary rocks of the Orea group (Eocene to Paleocene age) and the lithology of the group is sedimentary, consisting primarily of sandstone and siltstone (Wilson et al., 2015). The volume is estimated between 66 and 150 Mio.m³ (14 to 113 Mio.m³ according to Schaefer et al. (2024); Tab. D2 and App. D).

2.1 Portage

Portage Glacier is a lake-terminating glacier located at the northern part of the Kenai Peninsula, around 7.5 km southwest of Whittier, Alaska (Fig. 1A and Fig. 2). The glacier flows northeast and extends from an ice field at 1430 m a.s.l. to around 60 m a.s.l.. At the north end of the glacier, where the glacier calves into Portage Lake, there are two instabilities. We focus on the larger and more active of the two, laying farther up-glacier, between 200 and 1100 m from the 2021 terminus. The instability shows clear signs of deformation including tension cracks, a main scarp, a talus source area, and antiscarps (Higman et al., 2023). Rockfall activity has been observed at the site and surficial streams on the slide disappear into the subsurface (Higman et al., 2023). InSAR data suggest the landslide moved between 2016 Alsek—the terminus has not yet retreated past the landslide area. At the other four sites—Barry, Yale, Tyndall, and Grand Plateau—the glacier has retreated past most or all of the landslide area, and 2022 (Schaefer et al., 2024). The instability is located in Chugach flysch (Upper Cretaceous age) and the lithology is sedimentary, composed primarily of metagraywacke and metasiltstone (Wilson et al., 2015). The instability has a volume of around 11 to 35 Mio.m³ (5 to 19 Mio.m³ according to Schaefer et al. (2024); Tab. D2 and App. D).

2.1 Barry

Barry Glacier is a tidewater glacier flowing southwest into Barry Arm in Prince William Sound, around 50 km northeast of Whittier, Alaska (Fig. 1A and Fig. 2). The glacier flows from an accumulation area in a large ice complex in the Chugach Mountains at 2700 m.a.s.l. to sea level. The region around the glacier terminus is very dynamic. There are a number of instabilities to the northwest and southeast of the terminus. We focus on the largest instability, which is characterized by anti-these instabilities now border lakes or fjords. The sites have thus been impacted by glacier mass loss to varying degrees and in different ways, and normal-scarps, a main scarp, and a talus slope area (Higman et al., 2023). Multiple studies have confirmed the movement of this landslide since 2000 (Dai et al., 2020; Schaefer et al., 2024). Like Portage, the Barry instability is located in Chugach flysch. As of 2021, around half of the landslide toe was buttressed by the glacier, though the glacier has been retreating past the instability since 2010. The Barry instability is the second largest in this study, with an estimated volume of 188 to 500 Mio.m³ (117 to 564 Mio.m³ according to Schaefer et al. (2024); Tab. D2 and App. D).

2.1 Yale

Yale Glacier is a tidewater glacier terminating in College Fiord in Prince William Sound, approximately 70 km northwest of Valdez, Alaska (Fig. 1A and Fig. 2). It flows from a large glacier complex in the Chugach Mountains at around 3600 m.a.s.l. to sea level. Within 2 km of the present-day terminus, there are three instabilities. We focus on the largest of the three, which has a volume between 255 and 750 Mio.m³ (145 to 1025 Mio.m³ according to Schaefer et al. (2024); Tab. D2 and App. D). The instability is characterized by anti-therefore showcase a range of possible settings. All study sites are large landslides in sedimentary or metamorphic rock. Further description, including why each site was of particular interest, is found in Appendix A, and normal-scarps, a talus slope area, shear zones, and tension cracks (Higman et al., 2023), and movement of the landslide has been confirmed with InSAR (Schaefer et al., 2024). As with the other nearby instabilities, the lithology of this site is Chugach flysch. Debuiting of the landslide began around 1977, but it took until 2021 for the terminus to completely retreat past the toe area.

2.1 Columbia

Columbia Glacier, located around 35 km northwest of Valdez, Alaska (Fig. 1A and Fig. 2), is likely one of the most well-known glaciers worldwide due to its striking retreat over the past decades. The highest reaches of the glacier are nearly 3700 m.a.s.l. in the Chugach Mountains and it flows to the south down to sea level in Prince William Sound. Near the present-day terminus of Columbia Glacier, there are several instabilities to the north. We select the instability which is closest to the terminus (between 500 and 1800 m in 2021) and which could pose the largest hazard in the coming decades. The instability is characterized by tension cracks, normal-scarps, a talus slope, and a lake which drains periodically (Higman et al., 2023). InSAR results from Schaefer et al. (2024) suggest the landslide moved between 2016-2022. The lithology of the instability is Chugach flysch. It has a volume of approximately 44 to 150 Mio.m³ (17 to 111 Mio.m³ according to Schaefer et al. (2024); Tab. D2 and App. D).

2.1 Tyndall

Tyndall Glacier is located in the St. Elias mountain range and terminates at sea level in Taan Fiord, around 110 km northwest of Cordova, Alaska (Fig. 1C and Fig. 2). The glacier is bordered by some of Alaska's tallest mountains, with an accumulation area reaching up to 5290 m a.s.l.. There are a number of instabilities near the terminus of Tyndall Glacier. We select the one that failed catastrophically in 2015, which had a volume of 63 Mio. m³ and caused a tsunami with 193 m runup (Higman et al., 2018). The remaining sliding mass is around 100 Mio. m³ (Tab. D2 and App. D). This site is thus distinct from the others because it has already experienced a catastrophic failure. The instability at Tyndall is located in the Kulthieth Formation, a sedimentary lithology from the Eocene composed of conglomerate mudstone (Wilson et al., 2015). As of 2021, the glacier buttresses the length of the landslide toe. After a rapid retreat in the late 1980s, the glacier terminus was up-valley with respect to the landslide but has been stable or slowly advancing since the early 1990s. an overview of the sites can be seen in Figures 1 and 2. Note that we use the terms "landslide" and "instability" interchangeably throughout this publication.

2.1 Alsek

Alsek Glacier is located in southeastern Alaska, around 100 km from Yakutat (Fig. 1D and Fig. 2). Alsek Glacier flows from an elevation of 2420 m a.s.l. down to 60 m a.s.l.. The glacier terminates in Alsek Lake, which has grown from a few square kilometers in the 1950s to about 75 km² today as the glacier has retreated (Loso et al., 2021). Between 3.5 and 5 km up-glacier from the 2021 terminus, an instability with a volume between 19 and 50 Mio. m³ (Tab. D2 and App. D) is found on the eastern side of a nunatak. The failure is characterized by a large head scarp which extends around 1 km laterally. The instability at Alsek Glacier is found in volcanic rocks of the Chugach accretionary complex, a metamorphic lithology from the Upper Cretaceous (Wilson et al., 2015). Gneiss, migmatite, and schist are the primary rock types (Wilson et al., 2015).

2.1 Grand Plateau

Grand Plateau Glacier is located in southeast Alaska, around 120 km from Yakutat (Fig. 1 D and Fig. 2). It is a very large glacier, spreading over an area of 237 km² and spanning an elevation range of nearly 4600 m. The glacier currently terminates in three different lakes. We focus on the southeastern branch, where an instability with a volume of 50 to 150 Mio. m³ is present (Tab. D2 and App. D). The instability at Grand Plateau Glacier is located on an east-facing mountainside at the glacier left. The terminus began retreating past the instability around 2010, and the instability was completely debuttressed in 2022. It displays signs of movement through scarps, and like Alsek, it is located in volcanic rocks of Chugach accretionary complex.

3 Data & Methods

In order to understand how glacier thinning and retreat control the mobility may control the motion of the investigated landslides, we analyzed their slope deformation in response to glacier and environmental changes over the past 40 years. Specifically, we characterized their deformation from a combination of automatic and manual feature tracking on satellite optical

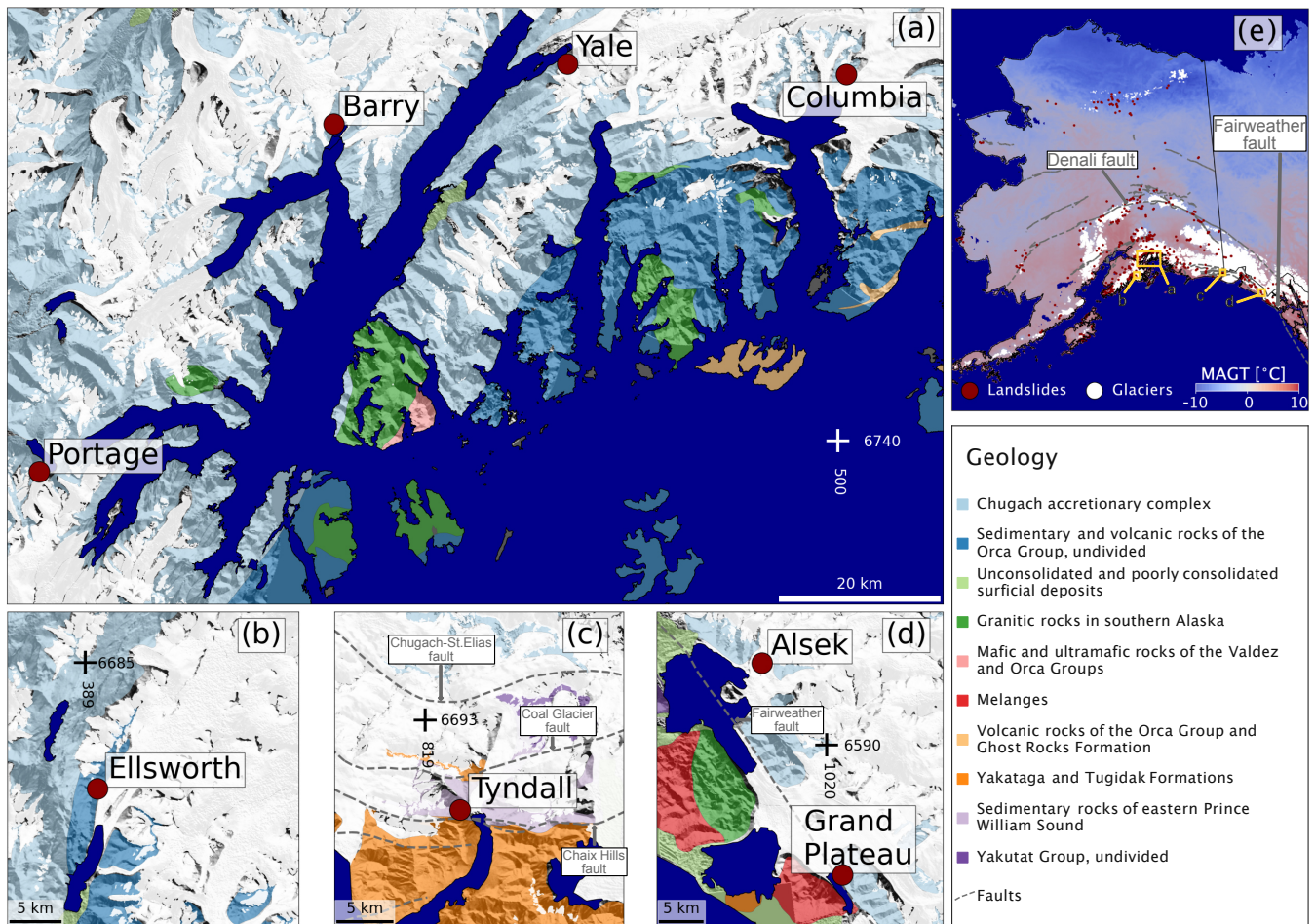


Figure 1. Overview of the [study sites of interest](#). Panels A-D (see panel E for location within Alaska) show the geology of the region (Wilson et al., 2015), with the legend at bottom right. [Sites of interest](#)—The study sites are labeled with dark red points. [Ocean](#)—Panel E shows the mean annual ground temperature (MAGT) (Obu et al., 2018), along with sites from Higman (2022) (red dots), glacierized area from RGI Consortium (2017) (white area), and faults from U.S. Geological Survey and Alaska Department of Natural Resources (2024) (gray dashed lines). Ocean area (dark blue) is from © OpenStreetMap contributors 2024. Distributed under the Open Data Commons Open Database License (ODbL) v1.0. A 2000s digital elevation model is used as a background layer (Hugonnet et al., 2021). [Panel A](#) larger version of panel E shows is in the [permafrost probability](#) (Obu et al., 2018), along with all sites from Higman (2022) (red dots), the glacierized area from RGI Consortium (2017) (white area), and faults from U.S. Geological Survey and Alaska Department of Natural Resources (2024) (blue dashed lines) [Supplementary Materials](#).

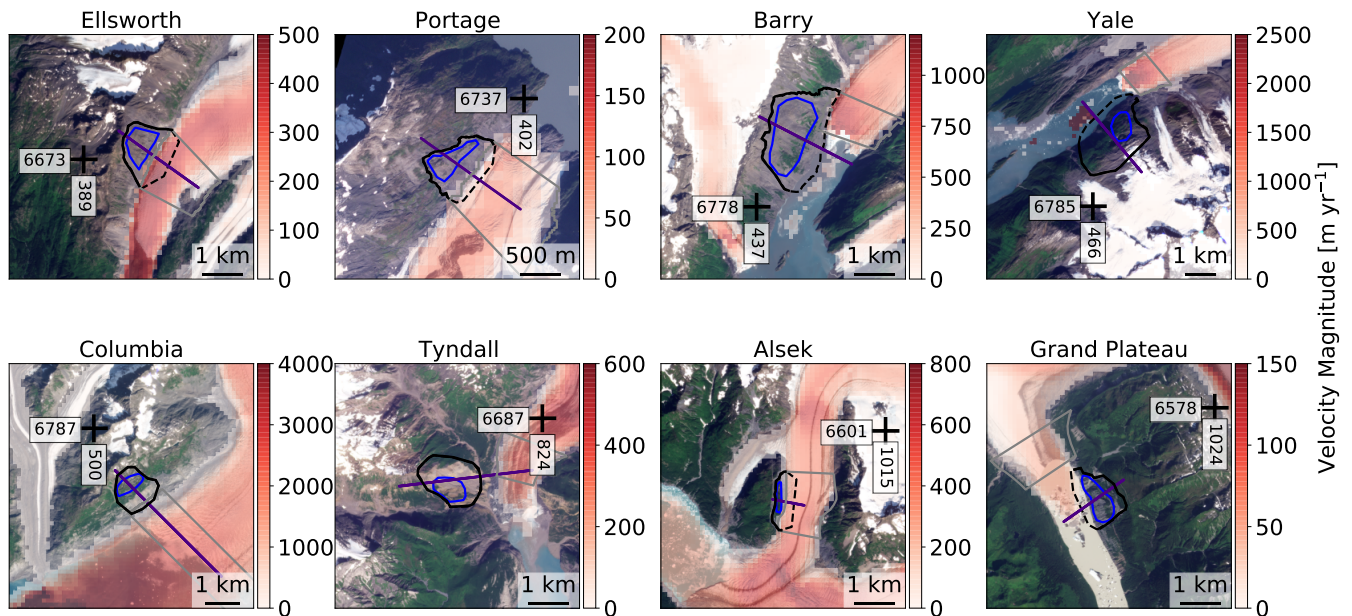


Figure 2. Satellite imagery from August 2023 over the eight investigated sites (see Fig. 1 for location). Images © 2023 Planet Labs PBC. Instability outlines are shown in black, and where dashed lines provide an estimate for the instability extents that are not visible at the surface (estimated subglacial or submarine instability extents). In the text, the resulting area is referred to these outlines as “instability polygons” (see App. D for a description). The “active areas” (described in Sect. 3.1) are shown in white, and the cross section (described in Sect. 3.2 and App. C) is plotted in orange. The instability-adjacent-glacier (IAG) polygon (see Sect. 3.2 and App. C) is plotted in red as a gray outline. Red shading represents the glacier speed from ITS-LIVE (Gardner et al., 2023), note that scales differ by more than one order of magnitude. Coordinates crosses refer to the UTM 6 projected coordinate system. The source of all images is Planet Labs PBC.

imagery, and combined this with several parameters describing glacier change. We determined glacier retreat rates by mapping yearly terminus positions and quantified glacier thinning rates from digital elevation model (DEM) differencing. From these data, we evaluated whether any acceleration of the paraglacial landslide coincided with changes in glacier behavior. Finally, to gauge the importance of the glacier-related controls, we evaluated time series of precipitation and seismicity as possible alternative drivers of landslide mobility co-drivers of landslide deformation. The details of the individual datasets and methods applied are presented in the following sections.

3.1 Landslide displacements

We retrieved landslide velocities from the ITS-LIVE annual mosaics (Gardner et al., 2023). The dataset was originally developed to map glacier flow, but it extends beyond the glacier boundaries and allows for applications on neighboring nearby slopes. ITS-LIVE data is generated from Landsat 4-8 image pairs and processed using the autonomous Repeat Image

Feature Tracking algorithm (auto-RIFT; (Gardner et al., 2018)). ~~For each year between~~ Between 1984 and 2022, the following relevant parameters are available ~~each year at 120 m-resolution~~: velocity magnitude, velocity components in the x- and y- directions, and an estimate for the uncertainty in the velocity. ~~The resolution of the product is 120 m. While the resolution is not enough to distinguish accelerations of small-scale features, it is sufficient to determine velocity changes at the scale~~ Because its primary use is on glaciers, the ITS-LIVE processing parameters are optimized for velocities that are much higher than for typical landslide motion. Additionally, the relatively coarse resolution of the dataset means that small displacements cannot be detected accurately. ITS-LIVE is thus expected to perform better for larger and fast-moving landslides, where surface features and resulting displacements are larger. Small changes or displacements of landslide are by no means irrelevant, but the resolution seems adequate for investigating the slope-wide responses of the landslides ~~we consider~~ to glacier changes.

~~For each year in~~ To retrieve landslide velocities from the ITS-LIVE ~~dataset data~~, we extracted the velocity and uncertainty over the "active area" of the instability (~~see below~~). ~~The median velocity and uncertainty were computed over this area, thus~~ creating to create an annual time series. The active area was delineated by selecting velocity pixels which fell within the instability polygon (see Fig. 2 for definition) and which showed movement in the ~~1984-2022~~ 1984–2022 ITS-LIVE velocity magnitude data (Fig. 3). ~~We~~ In some areas, the ITS-LIVE data appears to show "leakage" of the glacier signal to glacier-adjacent pixels, which may result from i) uncertainties in the glacier margins, ii) temporal inconsistencies between the glacier margins and the ITS-LIVE data, or iii) a large window size used during image cross-correlation. This leaked signal typically extends 1 to 2 ~~pixels (i.e. up to 240 m) away from the glacier and thus affects a small portion of the landslides' extents. When defining the active area, we excluded glacier pixels as defined by the RGI Consortium (2017) inside the RGI Consortium (2017) outlines, as well as any pixels adjacent high-velocity pixels moving parallel to the glacier which had a high-velocity compared to the instability and moved parallel to the glacier, and thus do not expect this leakage to impact our results.~~ At sites where no motion was ~~detected~~ shown by ITS-LIVE, we selected pixels over the area where most deformation is seen from satellite images.

~~We supplement the data from~~ Since we focus on landslide evolution over several decades—going back to the start of the satellite era—we leverage yearly and multi-year velocities to characterize landslide changes. The usage of annual data may result in the loss or smoothing of the signal, especially during times of rapid movement, and it does not allow us to see seasonal effects. However, this temporal resolution allows for characterization of long-term trends and interannual changes. Prior to 2000, the ITS-LIVE with measurements from manual feature tracking on the Landsat data at approximately five-year time steps. We do this for two reasons: i) pre-2000 ITS-LIVE data has relatively high uncertainty and we question its reliability and ii) visual inspection of the Landsat images over longer time steps (5 to 10 years) often show clearly visible changes that are not picked up by automatic feature tracking. We therefore high uncertainties due to the availability of only lower resolution satellite data during this time. For this reason, we employ manual feature tracking over 5-year time steps prior to 2000, and then use the ITS-LIVE data supplemented by the manual feature tracking between 2000 and 2022.

We selected cloud- and snow-free summer Landsat images on average every 5 to 6 years (some images were as little as 3 years or as much as 12 years apart) and manually mapped displacements indicating coherent motion ~~throughout across~~ the slope. We found this image spacing to provide large enough displacements to confidently map the changes (around 1 pixel or 30 m) and highlight the slope's temporal evolution. We classified movement as "coherent" or "slope-wide" if large vege-

tated patches within the instability polygon synchronously moved ~~in a given direction. Displacement or alteration downward~~
 275 ~~(changes~~ of isolated vegetation patches did not classify as movement~~in the analysis.~~). The “activation period” was defined
~~manually to be the timing of an initial pulse of significant, slope-wide deformation during our study period (Sect. 5.2).~~ For
 slopes that experienced catastrophic failure, no feature tracking was done ~~after the~~ during the time period containing the failure
 because the fundamental changes of the sliding mass make the pre- and post-failure slopes incomparable. ~~The velocity was~~
~~computed by determining the average distance travelled by individual features over the time period covered by two consecutive~~
 280 ~~images, and by then dividing that distance by the corresponding~~ For each landslide feature indicating slope-wide movement
~~(e.g. crack opening, displacement of vegetation patches), we took around three to five measurements of the distance moved~~
~~between two images. The median of these measurements, divided by the~~ number of years between the images, gives the slope
speed for that period.

3.2 ~~Surface~~ Glacier elevation changes

285 To quantify glacier thinning or thickening, ~~as well as landslide subsidence or thickening,~~ we computed the differences between
 seven different DEMs: a 1960s DEM from Berthier et al. (2010), a 1978 DEM from Dehecq et al. (2020), and the 2000, 2005,
 2010, 2015, and 2020 DEMs from Hugonnet et al. (2021). Both the 1960s and 1978 DEMs are composites from different years
~~-(see Tab. B1 in App. B).~~ The DEM by Berthier et al. (2010) was generated from historical USGS maps produced between
 1948 and 1972, although for the glaciers of interest the information stems primarily from a single year (small portions in the
 290 accumulation area might stem from another year). The DEM has a spatial resolution of 40 m and ~~for simplicity~~ we will refer to
 it as the 1960s DEM. The DEM from Dehecq et al. (2020) is generated from declassified analog satellite stereo-images from
 the American reconnaissance program Hexagon (KeyHole-9) and covers the late 1970s. Here, the dates range from 1977 to
 1980, but we will refer to this as the 1978 DEM. This DEM has a spatial resolution of 48 m. The DEMs from Hugonnet et al.
 (2021) cover the 21st-century and have a spatial resolution of 30 m. These DEMs were created by temporal interpolation of
 295 several repeat DEMs either generated from stereo-images from the Advanced Spaceborne Thermal Emission and Reflection
 Radiometer (ASTER) or retrieved from the ArcticDEM strip archive based on WorldView stereo-images (Porter et al., 2018).
 At each pixel, on average 40 independent ASTER or ArcticDEM elevations acquired in the period 2000–2019 are used to
 predict elevation at ~~the specific dates of~~ five-year intervals between 2000 ~~, 2005, 2010, 2015 or and~~ 2020.

Prior to extracting the elevation changes from the DEMs, we co-registered them ~~all~~ to the 2000 DEM to correct for shift
 300 and tilt misalignments. Horizontal and vertical shifts were removed following the iterative slope–aspect method of Nuth and
 Kääb (2011), then tilts were removed by fitting a 2-dimensional plane to elevation change residuals. Finally, we repeated
 the horizontal and vertical shift coregistration to remove sub-pixel shifts introduced by the tilt correction. This coregistration
 pipeline was performed using the ~~xDEM~~ xDEM package (xDEM contributors, 2024). The terrain used for coregistration was
 restricted to areas within 20 km of the glaciers of interest but excluding areas within 2 km of ~~their~~ the RGI Consortium (2017)
 305 outlines. There was a shift of 2 m on average, consistent with the offset reported by Berthier et al. (2010). The vertical reference
 of the 1960s DEM had to be transformed from the EGM96 geoid to the WGS84 ellipsoid. The vertical shifts resulting from
 the transformation were between –10 and 20 m, depending on the location in Alaska.

We computed surface elevation changes over the following time periods: 1960–1978, 1978–2000, 2000–2005, 2005–2010, 2010–2015, 2015–2020. ~~Note that no~~ Unfortunately, elevation data is not available for Ellsworth and Columbia in 1978 so ~~the~~
310 ~~changes over 1960–2000 were computed.~~ compared 1960 to 2000. We then examined the spatial distribution of the elevation changes throughout time, particularly over the glacierized area next to the landslide, and searched for periods of rapid thinning. The interpretation was aided by defining both a cross section and an instability-adjacent glacier (IAG) polygon (see Fig. 2 and See App. C for descriptions). Using the cross section, we extracted point values from the seven DEMs to create elevation profiles. Using the IAG polygon, we computed the median elevation change over the glacierized area near the instability in
315 different time periods.

3.3 Glacier terminus position

We used time series of glacier terminus positions mapped from Landsat images (1985–2022) to quantify glacier retreat and occasional glacier advance at yearly time steps. For Barry, Yale and Columbia, these data were already available until 2012 from McNabb et al. (2015), which provides manually-digitized terminus positions using all available Landsat images. For the
320 other sites (Ellsworth, Portage, Tyndall, Alsek, and Grand Plateau), we manually mapped the terminus positions on an annual basis using cloud-free summer images to minimize snow cover. The vast majority of the images used were taken between July and October, though occasionally a winter image was used if no summer image was available. A list of images used for delineation is found in the Supplementary Materials.

~~Glacier retreat rates were then calculated along the central flow lines of the glaciers. These centerlines~~ We calculated retreat
325 rates along the glacier centerlines, which were taken from RGI v6 (RGI Consortium, 2017), ~~though we had to manually extend them down valley.~~ The centerlines had to be manually extended down-valley to account for ~~the larger glacier extents during the early years~~ larger glacier lengths during the start of our study period (RGI outlines represent the glacier states around the year 2000). In some cases we manually refined the automatically generated RGI centerlines to more accurately represent the glacier and valley shapes. Finally, we calculated ~~the~~ retreat by intersecting the centerlines with the glacier terminus positions,
330 and cumulating the retreat relative to the largest glacier extent.

3.4 Supporting glacier and environmental data

3.4.1 Ice thickness

We used the two global ice thickness datasets by Farinotti et al. (2019) and Millan et al. (2022) to determine the valley topography below the glacier, put ice thinning rates into context, and estimate the ice remaining in front of the landslides.
335 ~~Two ice thickness products were used in order to increase the robustness of the result and to~~ Rather than rely on a single product, we used both to obtain a range of possible values. Both Farinotti et al. (2019) and Millan et al. (2022) ~~determine ice thickness using surface characteristics,~~ derive ice thickness from surface characteristics such as elevation, slope, and ice velocity. Farinotti et al. (2019) ice thickness dates refer to the glacier outlines from RGI Consortium (2017) version 6, while Millan et al. (2022) corresponds to the ~~year 2017–2018~~ years 2017–2018.

340 The elevation of the glacier bed was determined by subtracting the given ice thicknesses from a 2015 DEM (Hugonnet et al., 2021). ~~Note the~~ The usage of a DEM that does not correspond to the year of the ice thickness introduces some error, but we expect this to be minor ~~in comparison as compared~~ to the ice thickness uncertainty. ~~Using the defined cross sections (See For both datasets, we used the cross section (App. C) ; we extracted to extract the bedrock elevation resulting from each thickness dataset. Similarly, we computed the median thickness within the and the~~ IAG polygon (see ~~See~~ App. C) ~~from both datasets to~~
345 compute the median thickness.

3.4.2 Meteorology

~~We extracted~~ To determine the importance of non-glacier related environmental changes, we analyzed time series of precipitation. However, determining an appropriate time scale for this is challenging, as landslides can be activated by both heavy, short-duration precipitation events as well as extended periods of particularly wet conditions. We used time series of monthly temperature
350 and precipitation from ERA5 reanalysis data (Hersbach et al., 2018) to determine ~~if~~ how meteorological changes may correlate with landslide activity. For each site, we selected the grid cell ($0.25^\circ \times 0.25^\circ$) encompassing the instability and retrieved the monthly values from 1979 until 2022. We averaged ~~monthly temperature values and summed monthly precipitation values~~
temperatures and summed precipitation totals to get annual values.

We inspected the data for changes in meteorological conditions which may explain increased slope activity, such as particu-
355 larly rainy months or years. To do so, we computed the annual precipitation anomaly against a reference time period from 1980 to 2009 and evaluated this against the mean annual air temperature (MAAT) to identify potential “wet and warm years” that could have provided particularly high water inputs. We looked for years in which anomalously high precipitation correlated with increased landslide movement. Because the yearly time scales only provide a crude assessment, we also determined the average and standard deviation of ~~the monthly precipitation. We then~~ monthly precipitation and investigated if periods of in-
360 creased slope activity corresponded to times with ~~particularly high precipitation~~ anomalously high precipitation at the monthly level (exceeding two standard deviations above the mean). ~~In addition to the monthly analysis, we used the pymannkendall package (Hussain and Mahmud, 2019) to determine long-term trends in the yearly time series.~~

3.4.3 Seismology

We used the USGS Earthquake Catalog to extract all seismic events in the study area between 1980 and 2023 (U.S. Geological
365 Survey, 2023). We selected earthquakes which were within 100 km of a study site and that had a magnitude ≥ 4 . Magnitude 4 is ~~widely~~ considered to be the threshold at which earthquakes can cause landslides (Keefer, 1984). However, we acknowledge that pre-1980s events, ~~as well as repeated in addition to~~ smaller earthquakes, may have caused rock damage that ~~permanently destabilized the slope could contribute to a slope destabilization.~~

We ~~are interested in quantifying seek to quantify~~ the effect of seismic activity on slope stability, since ~~seismic activity~~
370 earthquakes may induce rock mass fatigue and promote failure (Gischig et al., 2016). ~~Using the above dataset, we estimate an intensity of the seismic events at the location of the investigated instabilities. To do so, we, though shaking can influence rock strength in a variety of ways, ranging from decreased to increased strength (Brain et al., 2021). We~~ first calculate the energy E

released by each earthquake. For an earthquake with magnitude M , this is given by $E = 10^{(5.24+1.44*M)}$ (Earthquake Hazards Program, 2024). We then estimate ~~a location-specific~~ an intensity I ~~, which we define of the seismic events at the location of~~
 375 ~~the investigated instabilities, defined~~ as the quotient of the earthquake energy E and the square of the distance d between the instability and the earthquake epicenter:

$$I(t) = \sum_t \frac{E(t)}{d^2} \therefore \quad (1)$$

~~Here, where~~ t is the time ~~since 1980, and the summation is meant to represent over one year. The summation thus represents~~
 the cumulative energy experienced at ~~each site up to the given point in time~~ a site during a particular year. We inspected the
 380 resulting time series for periods where the ~~cumulative~~ seismic intensity increased sharply, and assessed whether such periods coincided with increased slope activity.

4 Results

To understand how glacier retreat controls landslide activity, we analyzed landslide displacements and glacier behavior from the early 1980s to present-day. Half of the studied landslides—Barry, Yale, Tyndall, and Grand Plateau—are currently situated
 385 adjacent to lakes or fjords which were occupied by glaciers in the 1980s. The other half of the landslides—Ellsworth, Portage, Columbia, and Alsek—still have contact with the glacier along the whole landslide toe. In the following, we first describe the most important stages of the landslide evolution at each site, and then describe the glacier activity during these stages. We summarize the temporal connections between the landslide and glacier changes, and present the findings of both the meteorological and seismic investigations.

390 4.1 Landslide evolution

Seven out of eight sites displayed clear down-slope movement between 1984 and 2022 (Fig. 3), ~~moving at average speeds of~~
 ~~~ 3.4 to ~ 8.6 m yr $^{-1}$.~~ At six of these sites, the combined use of ITS-LIVE data and manual feature tracking revealed distinct
 periods of acceleration or large surface changes (Fig. 4 ~~); During these times~~ and Fig. E1 in App. E). The landslides moved
at average speeds of ~ 2.8 to ~ 8.7 m yr $^{-1}$ in the period 2000–2022 and up to a maximum velocity of 79 m yr $^{-1}$ (Ellsworth).
 395 During periods of acceleration, the landslide velocities from ITS-LIVE increased ~~by up to~~ a factor of two (Grand Plateau)
~~to seventeen (Ellsworth) 9~~ compared to the average velocity ~~in the five years prior to the acceleration~~ between 2000 and
2022. Manual feature tracking, on the other hand, gave maximum velocities up to 7 times higher than the long-term average
(1984–2022). In the following, we will discuss the behavior of individual landslides in more detail.

At Tyndall and Yale, landslide activity began as early as the 1980s and 1990s, respectively. At Tyndall, a 60 m-wide crack
 400 opened at the top of the landslide between 1987 and 1990 (Fig. 4 ~~e1 and Fig. E1Cf~~). Further disintegration of the slope followed, including slope-scale motion starting in the 2000s, culminating in ~~the catastrophic failure of a catastrophic failure in~~ 2015.
~~While around~~ Around 60 Mio. m 3 fell into the fjord ~~, another 100 Mio. m 3 remain and another 100 Mio. m 3 remained~~ on the
 slope and have continued moving ~~slightly~~ since 2015. At Yale, manual feature tracking ~~between 1989–1995 shows~~ showed that

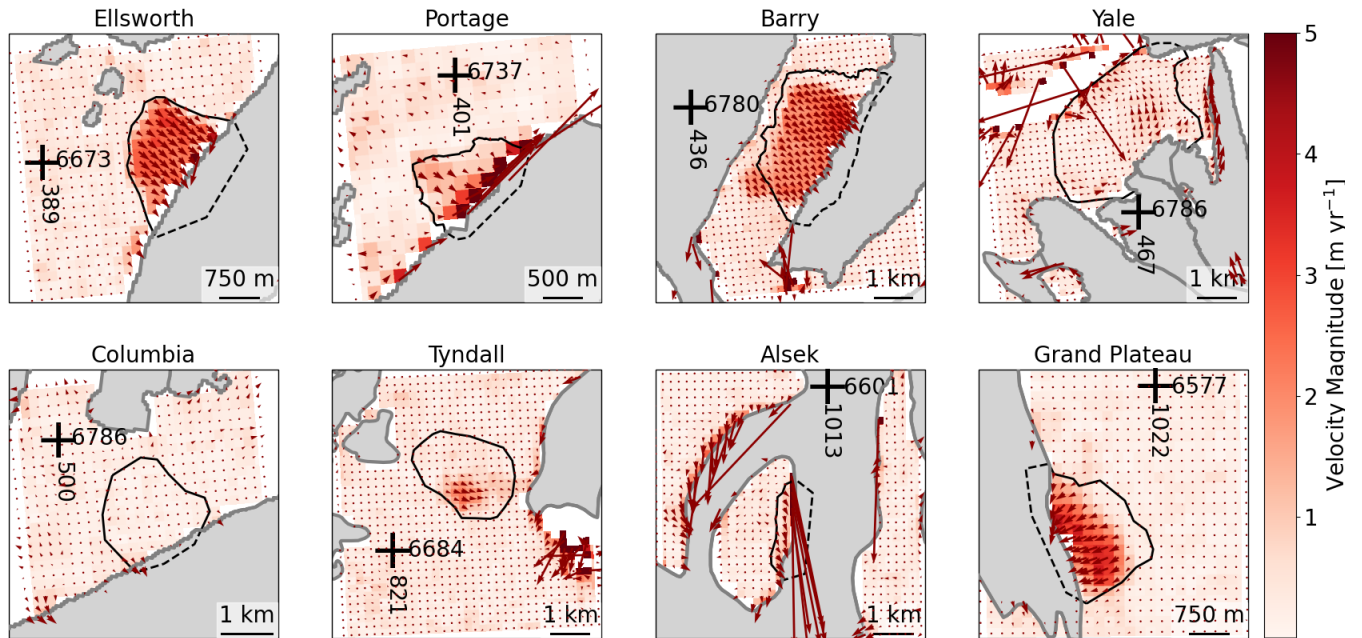


Figure 3. Average (1984-2022) displacement vectors and velocity magnitude derived from ITS-LIVE data. Glaciers are shown in gray (outlines from RGI Consortium, 2017) and black outlines mark the instability polygon (cf. Fig. 2). Coordinate crosses are given in UTM 6.

the landslide experienced a sudden pulse of movement [between 1989 and 1995](#) (Fig. [4b1](#) and [Fig. E1Bd](#)), with surface features
 405 being displaced by around 75 m. The location of these surface displacements coincides with the [area of increased activity](#)
[visible region of highest velocity](#) in the ITS-LIVE data (Fig. 3). [Based on The](#) manual feature tracking [, we did not detect](#)
[not reveal](#) any visible motion after this period, though the ITS-LIVE data indicates a small velocity increase around 2010 (see
[Fig. 4b1](#)), which may suggest [slight](#) ongoing creep.

At four other sites (Barry, Grand Plateau, Alek, and Ellsworth), activity started between 2000 and 2010. The Barry landslide
 410 accelerated between 2004 and 2010 (Fig. [4a1](#) and [Fig. E1Ac](#)). Manual feature tracking indicates the movement started between
 2009 and 2010, while ITS-LIVE data shows the acceleration beginning after 2008 and the velocity peaking around 30 m yr^{-1}
 between [2010-2012](#). [Between 2013-2016](#) [2010 and 2012](#). [Between 2013 and 2016](#), the landslide slowed to around 10 m yr^{-1}
 before the velocity stabilized at approximately 2 m yr^{-1} in 2017. This acceleration displaced large parts of the landslide by
 around 200 m [in total](#) between 2004 and 2021.

415 During the same time (beginning of the 2000s), a $\sim 45 \text{ m}$ -wide crack opened at the top of the Grand Plateau landslide (Fig.
[4d1](#) and [Fig. E1Dh](#)). Manual feature tracking narrows down the movement onset to between 2007 and 2009. ITS-LIVE data
[reveal that slope-scale motion continued](#) [show that the slope moved at a constant velocity of around \$2.5 \text{ m yr}^{-1}\$](#) between 2010
 and 2022, [albeit movement appears to have stopped around 2018, with the exception of an active drainage area in the north.](#)
[For both Barry and Grand Plateau glaciers, we observed small slope failures along one side of](#) [though manual feature tracking](#)

420 indicates much larger displacements. We suspect that this discrepancy is due to the ~~valley-as-the glacier retreated up-valley.~~
slope appearance changing drastically and significant vertical motion, both of which pose challenges for the feature tracking
algorithm.

At Alsek Glacier, the ITS-LIVE landslide velocity peaked at ~~over 20 m yr⁻¹~~ around 10 m yr⁻¹ in 2008 and a 60 m wide crack opened between 2006 and 2008 (Fig. 4h+g). After this event, ~~only slight displacement (<30 m) occurred the landslide~~
425 velocity decreased to around ~5 m yr⁻¹ between 2010 and 2021. A similar phenomenon is observed at Ellsworth Glacier: The landslide accelerated dramatically in 2009, reaching velocities of ~~over~~ around 80 m yr⁻¹ and a cumulative displacement of 100 m between 2005 and 2010 (~~see~~ Fig. 4e+g). Later, between 2014 and 2021, the landslide continued to move, giving displacements around 30 m.

Finally, ~~two sites had minimal to no~~ at two sites, we detected limited or no movement over the study period. At Portage,
430 ~~no movement was detected by the~~ manual feature tracking did not reveal any motion (Fig. 4f+~~albeit b~~) although ITS-LIVE data indicates clear down-slope motion (Fig. 3). This suggests that there is slow but possibly continuous motion without any sudden, large changes. Indeed, looking at higher-resolution aerial imagery, substantial disintegration of the slope between 1996 and 2006 is visible (see Fig. E2 in App. E). At Columbia, no motion could be detected by ITS-LIVE (Fig. 3) or by manual feature tracking (Fig. 4g+e), despite the fact that the landscape shows signs of deformation.

435 4.2 Glacier evolution

All glaciers retreated between 1984 and 2022, with total retreat varying from ~~0.97 to 23.3 km~~ 0.97 to 23.4 km and average retreat rates ranging from 30 to 630 m yr⁻¹. ~~Two sites also showed Yale and Tyndall experienced short~~ periods of advance, but all the 2023 terminus positions are up-valley of the 1980s extents ~~in all cases~~. In accordance with the observed retreat, all sites thinned between 1960 and 2020, with average thinning rates ranging from ~~1.77 to 9.65 m yr⁻¹~~ 1.8 to 9.6 m yr⁻¹ (Tab. F1
440 in App. F, as well as Fig. 5). At four out of eight sites, periods with rapid glacier changes coincide with periods of landslide activity and slope acceleration (Fig. 4~~and Fig. E1~~), which we focus on in the following.

Between 1984 and 1988, Tyndall Glacier retreated up-fjord by 5 km. ~~This rapid retreat coincided with the crack opening at the head of the landslide (Sect. 3.1), which appears to have occurred,~~ and the feature tracking shows that the head scarp crack opened as the glacier terminus passed the landslide. ~~Following~~ After this dramatic retreat, the glacier terminus ~~advanced~~
445 ~~by around 700 m between 1995 and 2021. Near the landslide stabilized, fluctuating slightly around its new position. In 2021, it was around 800 m longer than its 1990 extent. At the terminus, the glacier thinned by 6.42 m yr⁻¹ on average 6.4 m yr⁻¹ between 1960 and 2000, and thickened by 0.56 m yr⁻¹ 0.6 m yr⁻¹ between 2000 and 2020 (Tab. F1).~~ In our study, Tyndall and Yale are the only two glaciers that showed; Fig. 4f). The glacier elevation near the landslide is currently around 200 m a.s.l., around 200 m less than in the pre-2000s period.

450 Aside from Tyndall, Yale is the only other glacier that experienced short phases of advance. ~~Like Tyndall, Yale experienced times of modest advance (a maximum of 170 m), around the year 2000 and after 2006. Here, the terminus advanced by about 130 m between 2004 and 2014~~ (Fig. 4b2d). Despite these short phases of stability ~~or advance~~, Yale Glacier retreated by around ~~1200 m~~ 1 km since the 1980s, a trend that was accompanied by rapid thinning. On average, Yale glacier thinned by

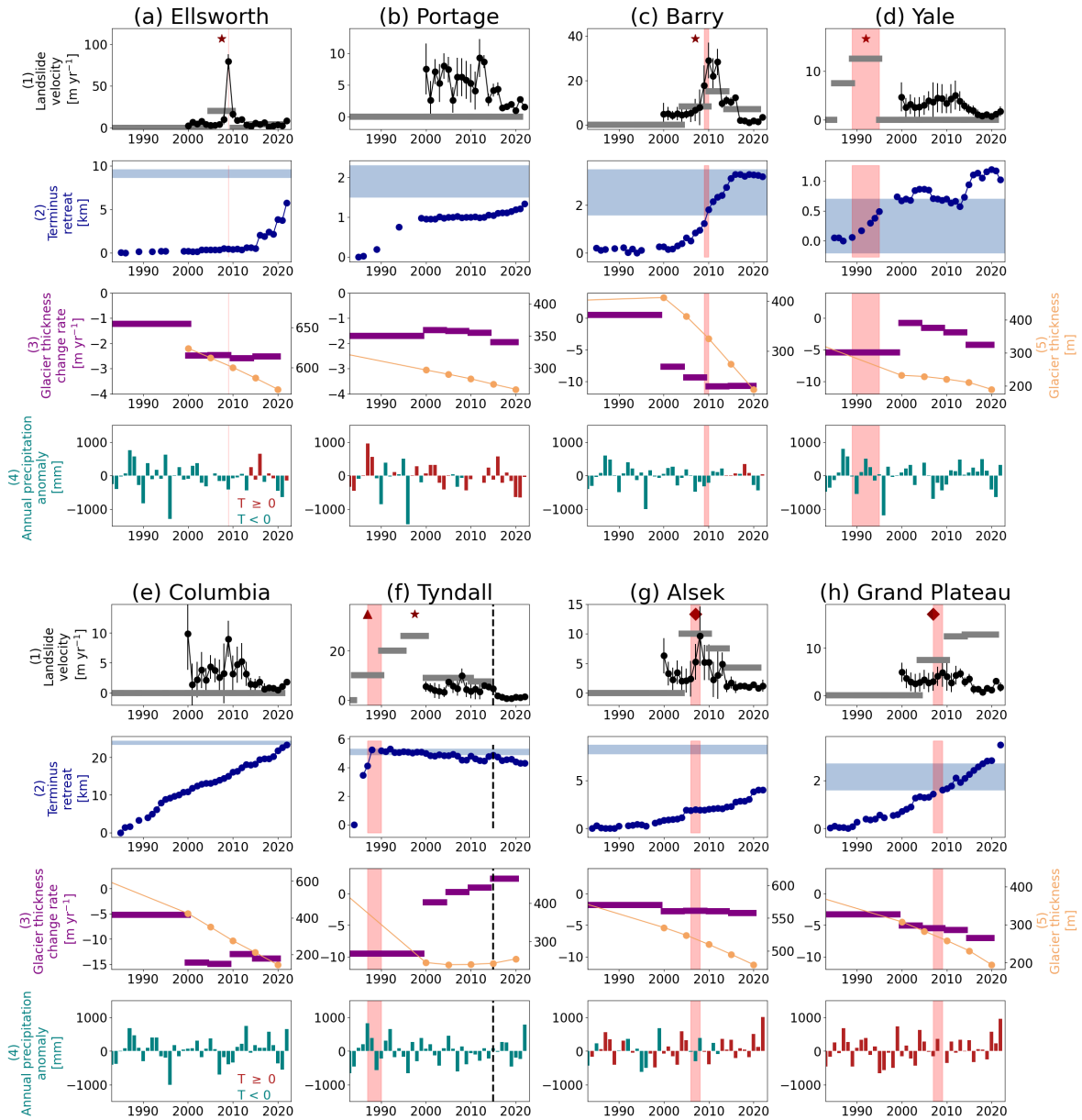


Figure 4. Landslide and glacier evolution at the [study sites of interest](#). **Top row Row 1:** Landslide velocities from ITS-LIVE (black circles, with [vertical lines showing the uncertainty estimate from ITS-LIVE estimates](#)) and manual feature tracking (gray bars). **Middle row Stars indicate onset of slope-wide deformation, triangles stand for crack opening, and diamonds mean both deformation and crack opening.** Row 2: Terminus retreat (dark blue) and location of the landslide along the glacier centerline (light blue shading). **Bottom row Row 3:** Glacier thickness change rates [within the IAG polygon \(see Fig. 2 for definition purple\)](#) based on data from [Dehecq et al. \(2020\)](#) and [Hugonnet et al. \(2021\)](#) absolute ice thickness (yellow; right hand axis) below the landslide. **Note at Ellsworth and Columbia Row 4:** annual precipitation anomaly from ERA5 ([Hersbach et al., 2018](#)) (relative to 1980–2009), the [Berthier et al. \(2010\)](#) DEM replaced the [Dehecq et al. \(2020\)](#) DEM where teal and red bars indicate a positive or negative MAAT. In all panels, light red shading indicates the onset of landslide movement. At Tyndall, the black dashed line indicates [a catastrophic the failure](#). Note the differing scales on the [y-axis for the individual sites y-axes](#).

3.29 m yr⁻¹ to 3.3 m yr⁻¹, the thinning rate being more than twice as high before the year 2000 than afterwards (5.52 m yr⁻¹ versus 2.18 m yr⁻¹ to 5.5 m yr⁻¹ versus 2.2 m yr⁻¹; Tab. F1). The increased thinning rate before 2000 also coincided with one of the most rapid periods of retreat: between 1989 and 1995, the glacier terminus retreated past the landslide area at around 70 m yr⁻¹, which is more than twice the long-term retreat rate of 30 m yr⁻¹. Again, just as at Tyndall, the strong retreat coincided with the main landslide displacement.

Barry Glacier retreated most rapidly up-fjord between 2003 and 2016, and slope motion began between 2009 and 2010 when the terminus was adjacent to the down-valley margin of the landslide. During this period of accelerated retreat, the terminus retreated, the retreat rate peaked around 230 m yr⁻¹, which was nearly three times higher than the average retreat rate over the 1985–2022 period. Near the landslide, the glacier thickened slightly (0.87 m yr⁻¹ on average) whole 1985–2022 period. In 2016, the terminus position stabilized at its current location near the up-valley end of the landslide, having retreated past ~75% of the landslide toe. Deformation of the terminus in response to the landslide movement is clearly visible from the ITS-LIVE velocity vectors (Fig. F1 in App. F). Aside from some mild thickening prior to 2000, while between (0.9 m yr⁻¹), Barry Glacier has experienced the second highest thinning rate of all study sites, thinning by 9.7 m yr⁻¹ per year between 2000 and 2020 the thinning rate was the second highest of the study (9.65 m yr⁻¹; 2020 (Figs. 4a2-c and 5). Since 2000, the glacier has lost around 350 m of ice near the landslide.

Similar to Barry, Grand Plateau Glacier also retreated around 3 km between 1985 and 2022, with and the current terminus position lies up-valley with respect to the landslide. Like Barry, slight deformation of the termini of both sites having retreated past most or all of the landslide. The thinning terminus in response to the landslide is visible (Fig. F1 in App. F). Thinning rates have been generally increasing since the 1980s (Fig. 4h). Near the landslide, the glacier thinning rate was 2.63 m yr⁻¹ to 2.6 m yr⁻¹ on average before 2000, and increased by a factor of two between 2000 and 2020. Since the 1980s, the retreat rate of Grand Plateau gradually accelerated as the glacier moved up-valley through the lake, but there was not one distinct period of acceleration. The glacier retreated around 90 m yr⁻¹ on average between 2007 and 2009, coinciding with both the glacier passing the down-valley margin of the landslide and the opening of the crack (Sect. 4.1). During this period, the retreat rate was equal to the 1984–2022 average velocity.

At Ellsworth and Alsek glaciers, both the retreat and thinning rates have increased over time (Fig. 4 and 5). Next to the landslide, Ellsworth Glacier's thinning rate was 1.22 m yr⁻¹ on average 1.2 m yr⁻¹ prior to 2000, which and increased by a factor of two between 2000 and 2020 (Figs. 4e3 and 5). This corresponds, corresponding to the time when the landslide accelerated. The position of the terminus terminus position was fairly stable in the a proglacial lake until 2014, when the tongue of the glacier began disintegrating and led to higher retreat rates. However, retreat rates increased. Currently, the instability was is still around 3 km from the terminus. Next and as much as 250 m of ice buttresses the landslide. At Alsek, the glacier adjacent to the landslide, Alsek Glacier thinned by 1.57 m yr⁻¹ to 1.6 m yr⁻¹ between 1960 and 2000, and by 2.85 m yr⁻¹ to 2.8 m yr⁻¹ between 2000 and 2020, a factor of 1.8 higher (Figs. 4h3 and 5). This brackets the period with the crack opening. Alsek Glacier's retreat through the proglacial lake followed a similar pattern: prior to 2000, the glacier Similarly, Alsek Glacier retreated around 45 m yr⁻¹ and the prior to 2000 and this rate increased by a factor of three since then. However, the terminus is still about 4 km down-valley from the instability.

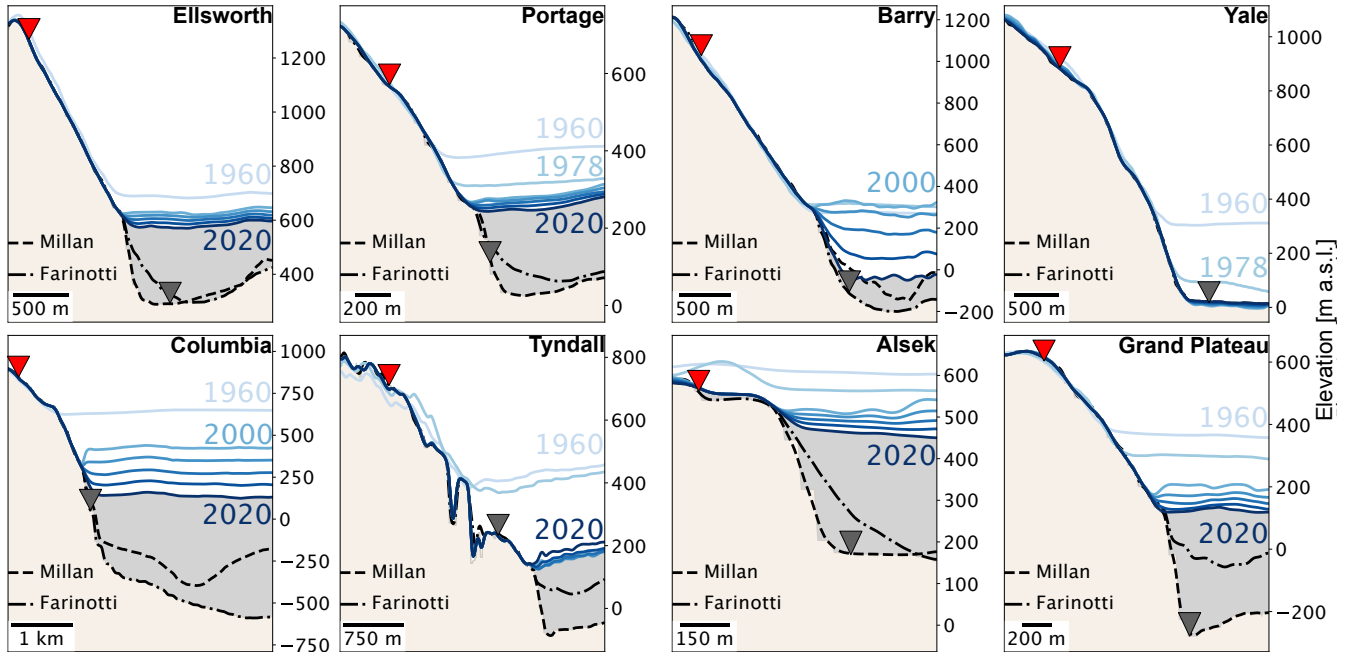


Figure 5. Cross sections through the landslide and glacierized area at each site. Bedrock (tan) and glacier areas (gray) are shown. Glacier surface elevations are plotted in progressively darkening shades of blue. Subglacial topography is given by two ice thickness datasets (Millan et al. (2022) and Farinotti et al. (2019)). Red and gray triangles mark the upper and lower bounds of the landslide, respectively. From the two bedrock estimates, the gray triangle was arbitrarily placed on the Millan surface. Note the horizontal and vertical scales vary between sites.

Both Portage and Columbia thinned during the study period, and the terminus is currently several hundred meters from the
 490 instability centerpoint (Fig. 4). With Along with Tyndall and Yale, Portage Glacier is one of three sites where the thinning
 rate was higher before 2000 than it was afterwards: Portage thinned at 2.2 m yr^{-1} before 2000, and at around ~~1.62 m yr^{-1}~~
 1.6 m yr^{-1} between 2000 and 2020. The glacier retreated rapidly (65 m yr^{-1}) through the proglacial lake between 1985 and
 2000, remained stable for around 15 years, and retreated at around 40 m yr^{-1} since 2015. Columbia Glacier, on the other hand,
 thinned by 5.2 m yr^{-1} ~~on-average~~ between 1960 and 2000, increasing by a factor of 2.7 to 14.1 m yr^{-1} between 2000 and
 495 2020. Here, steepening of the slope, likely due to glacier erosion, is clearly visible below the 1960s glacier surface (Fig. 5).
 Between 1985 and 2022, the glacier retreated up-fjord by over 23 km, or a rate of around 630 m yr^{-1} .

4.3 Landslide-glacier interaction

At four sites (Tyndall, Yale, Barry, Grand Plateau), we observed that landslide deformation began or increased as the glacier
 terminus passed the active area of the landslide. At Tyndall Glacier, the very rapid terminus retreat debutressed the landslide
 500 within a period of three years and a crack opened at the top of the slope when the glacier passed the landslide toe (Fig.
 E1C). A crack also formed at Grand Plateau landslide where, as the terminus retreated past the down-valley margin of the

landslide, slope-wide deformation began (Fig. E1D). The same is true for Barry Glacier: when the terminus was adjacent to the down-fjord edge of the instability, the whole slope moved significantly and a headscarp formed (Fig. E1A). At Yale Glacier, the movement was more localized and involved only the active area rather than the entire instability, but the surface features displaced down-slope as the terminus passed the active area (Fig. E1B).

Landslide features and glacier terminus position during movement onset for sites where the terminus has passed the landslide. The year of acquisition of the individual satellite images is given at upper left. The panel at far right shows a zoomed version of the previous panel (shown by the black dashed box). Solid lines refer to the year at upper left in each image and for subsequent years, dashed outlines refer to the first time period (image at far left). Arrows highlight the formation of a head scarp (1), downward displacement of vegetation patches (2), downward displacement of surface features (3), widening of a crack (4), and the formation of a crack (5). Panels A-D refer to Barry, Yale, Tyndall, and Grand Plateau, respectively. Background images are Landsat 4-7 courtesy of the U.S. Geological Survey.

At the four sites where the terminus is still down-valley with respect to the instability (Portage, Ellsworth, Alsek, Columbia), we see varying behavior of the landslides. At Portage Glacier, the landslide moved slightly, but with a constant velocity and without a distinct acceleration. At Ellsworth and Alsek, the landslides had sudden, large accelerations that do not coincide with an obvious change in the glacier. However, the glacier thinning rates of both sites increased by about a factor of two over the same period as the landslide accelerations. On the contrary, thinning at Columbia Glacier increased by a factor of almost three but no landslide deformation was observed. While the link between glacier changes and landslide evolution is less clear at these four sites, we suggest that it could be related to glacier thinning.

4.3 ~~Landslide-environment interaction~~Other environmental controls

The results presented in the sections above suggest that glacier changes, especially rapid ~~retreat~~onset, may exert a strong control on landslide acceleration. To make this inference, however, alternative factors that might have initiated the larger slope displacements ~~need to~~should be ruled out. ~~Here below we address meteorology and seismicity as potential alternative explanations~~Below we address the possible influences of precipitation and seismicity.

4.3.1 Meteorology

~~Annual precipitation does not reveal any trend during the 1979-2022~~

We examined annual precipitation anomalies at all sites (Fig. 4). At most sites, precipitation totals during the year(s) of the landslide acceleration were close to the long-term average. At Ellsworth, Barry, Yale, Alsek, and Grand Plateau, small positive or negative precipitation anomalies were observed during the year(s) of the movement onset. However, in none of these cases were the anomalies exceptionally high when compared to the rest of the time series. All sites have relatively large precipitation totals, on average around 3200 mm yr⁻¹. The mean annual air temperature increased between 1979 and 2022 at all sites, on average by 0.04 °C yr⁻¹. At Tyndall, the year 1987 was characterized by a precipitation total over 800 mm above the long-term average—the largest anomaly in the time series. During this period of landslide activation, there were two years with above-average precipitation, followed by two years with below-average precipitation. Due to limited good-quality image

535 availability in the 1980s, there is large uncertainty in the exact onset of the landslide movement and thus the impact of the consecutive wet years on landslide initiation cannot be ruled out.

~~We examined the cumulative monthly precipitation~~ In addition to the annual time scale, we analyzed monthly precipitation totals at the six sites ~~which experienced landslide accelerations (Fig. ?? where landslide accelerations were observed (Figs. G1-G3 in App. G).~~ At Ellsworth, where the landslide accelerated between June and August 2009, yearly precipitation was below average. ~~However, (Fig. 4a). Amidst this dry period, however,~~ the precipitation during July 2009 was ~~as high as 293 mm, which is 80% above the average precipitation for July (Fig. G1.~~ July precipitation (293 mm). A connection between precipitation and landslide acceleration can thus not be ruled out in this case.

~~At Barry, Alsek, At Alsek and Grand Plateau glaciers, precipitation, some monthly~~ totals during the ~~years of the landslide acceleration were close to the long-term average. At Yale and Tyndall glaciers, one year during the landslide acceleration period (1989) was exceptionally dry, particularly in the first half of the year. At Tyndall, precipitation totals were well above average in November and December of 1987. Because landslide activation period were above average, but never exceeded two standard deviations above the mean. In the cases of Barry, Yale, and Tyndall, certain months did have anomalously high precipitation during the period of the landslide activation. However, because~~ we cannot determine the onset of the landslide movement more precisely, it is unclear if the ~~acceleration accelerations~~ might be related to ~~this large precipitation amount or if it these large precipitation amounts or if they~~ happened during a different time of the year. ~~Since it is fair to assume that the November and December precipitation fell as snow, one hypothesis could be that the landslide might have experienced increased loading. Taken together, however, the indications for a direct link between precipitation and landslide movement are weak.~~

~~Cumulative monthly precipitation at all sites which experienced a landslide acceleration during the study period. Thicker, darker blue lines correspond to the year (or years) during which the landslide accelerated. The light blue lines are all other years. The solid gray line corresponds to the mean monthly precipitation over the whole time period, and the gray dashed lines are two standard deviations above and below the mean. Note that y-axes differ between sites.~~

4.3.2 Seismicity

The seismic data were scrutinized to determine whether slope accelerations followed intense or prolonged seismic activity : ~~At four sites (Ellsworth, Barry, Yale, Tyndall), the landslide accelerations occurred during a period of low seismicity (Fig. ??).~~ At Alsek Glacier, a small earthquake occurred during the same time period as the ~~(Fig. H1 in App. H).~~ We did not observe a temporal correlation between high seismic intensity and landslide velocity during the years of landslide activation, nor did we observe increased landslide activity in the years following a particular seismic event. While we acknowledge that seismic shaking can cause rock damage which impacts landslide stability (see Sect. 5.2), the evidence here shows no direct link between specific seismic events and landslide acceleration. ~~The onset of movement at Grand Plateau Glacier appears to occur shortly after a small increase in earthquake intensity. Due to limited availability of satellite images, we cannot precisely constrain the onset of the landslide movement and thus do not know if a link might exist. However, both sites experienced even larger increases in seismic intensity in previous decades without leading to landslide movement, which seem to speak against~~

a possible causal link. We note that at most sites, large earthquakes occurred between 1980 and 1988. While these may have preconditioned the slope stability through fracturing, a clear link cannot be established.

570 Seismic intensity at the sites which experienced a landslide acceleration during the study period. For Ellsworth, where the acceleration can be pinpointed to a single year, that year is marked by a vertical dashed line. For other sites, the instability acceleration is marked by a shaded bar.

5 Discussion

575 The impact of glacier thinning on landslide destabilization has been investigated at several locations across the world, and there is general agreement that glacier thinning contributes to landslide destabilization (e.g., McColl and Davies, 2013; Glueer et al., 2019; Cody et al., 2020). So far however, most studies investigating glacial debuttressing have taken place at sites where the glaciers were land-terminating. Observations of landslides adjacent to retreating glaciers which give way to water are much less common (an exception is given by the studies of Kim et al. (2022) and Dai et al. (2020)), as is documentation of accelerations at such sites.

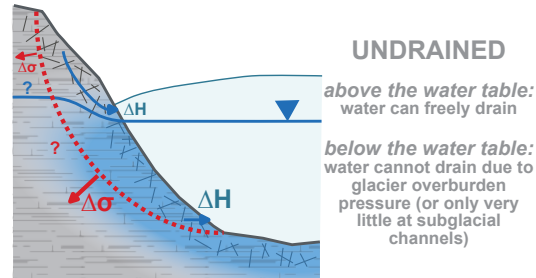
In this study, we investigated the response of paraglacial landslides to glacier changes over multiple decades. Our results show that ~~in four of eight cases (at Yale, Tyndall, Grand Plateau, Barry, all and Barry—all of which are lake- or marine-terminating glaciers), the landslides accelerated adjacent to lakes or fjords—the slope-wide deformation began~~ when the glacier retreated past the instability. Ellsworth experienced an increase in glacier thinning, but the landslide acceleration also coincided with an anomalously rainy month. At Alsek, we found a sudden activation which was preceded by an increase in glacier thinning. Finally, despite the continuous mass loss of both glaciers, Portage showed very little movement without a clear period of acceleration, and at Columbia, no movement was detected.

585 ~~The impact of glacier thinning on landslide destabilization has been investigated at several locations across the world. In the following, we discuss possible differences between the land- and water-terminating situations, evaluate the varying slope evolutions following destabilization situations at varying stages of retreat and evaluate the possible slope evolution following destabilization. We also compare our results to previously published work and propose future research perspectives.~~

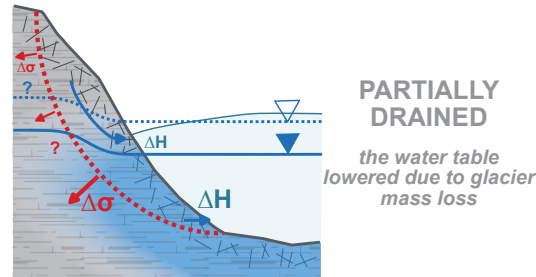
595 5.1 Landslide evolution in land- vs. water- terminating situations

As glaciers retreat, the hydrology and mechanics of the paraglacial slopes must adjust accordingly (Fig. 6). In temperate glaciers (ice at or near 0°C), water is readily available and it may flow on the surface, within, and below the glacier (Jansson et al., 2003). Englacial water storage can impact the pore pressure in neighboring slopes on seasonal timescales (Grämiger et al., 2020; Hugentobler et al., 2001), meaning that adjacent to the glacier, liquid water is present in subsurface pores and cracks and cannot drain due to the ice

a) glaciated conditions



b) during de-glaciation



c) upon glacier disappearance

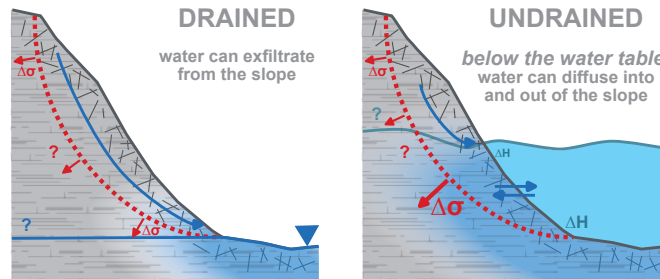


Figure 6. Conceptual figure outlining the changes to slope hydrology during different stages of glacier retreat (panels A and B), as well as in the presence of a proglacial lake or fjord after glacier disappearance (panel C). Rock mass is gray, glacier ice is light blue, and lake/fjord water is blue. The red line is the assumed failure plane of the landslide, and red arrows represent the slope displacement. The solid blue line and filled triangle indicate the current water table. The dashed blue line and unfilled triangle indicate the former water table. Blue arrows indicate where water can drain. “ ΔH ” is the overburden pressure from ice or water, and the size is representative of the magnitude. “ $\Delta\sigma$ ” is the pressure on the failure surface and the size represents the magnitude. The terminology of “drained” and “undrained” conditions follows Lacroix et al. (2020).

600 overburden pressure (Fig. 6a). The presence of water in the subsurface can be problematic for slope stability by decreasing the frictional forces and increasing pore water pressure within the slope, both of which contribute to instability (Blasio, 2011; Lacroix et al., 2020). Existing work has shown that during ice sheet retreat, groundwater can exfiltrate from the subsurface due to decreasing

ice overburden pressure (Ravier and Buoncristiani, 2018). Thus, as the glacier surface lowers, the water table in the slope moves to a correspondingly lower elevation (Fig. 6b) and the upper portion of the slope becomes “drained,” a term defined by Lacroix et al. (2020). In this case, excess pore water pressure cannot develop and this portion of the slope becomes stabilized. The part of the slope still under the water table, on the contrary, would remain saturated and “undrained.”

Upon complete disappearance of the glacier, the balance between the various other external forces (e.g. hydrological, mechanical, and geological) determines if the slope is stabilized or begins to move. The slope may be completely drained—in the case of a land-terminating landslide—or undrained in the case of a water-terminating one (Fig. 6c). In the former case, a new, stable equilibrium may be found as the slopes (re-)adjust to the changed boundary conditions. In the latter case, the slope remains saturated below the lake or fjord level and, similar to the glaciated case, hydraulic gradients can cause pressure changes along the failure surface, which impact slope stability (McColl, 2015). Such fluxes and pressure changes may cause further damage to rock which has already been weakened by glacier retreat and thinning (Grämiger et al., 2017, 2018). Additionally, the lower portion of the slope must support the mass above it, which it may not be able to do effectively when saturated. Thus in the case that an ice buttress is replaced by water, a precarious situation exists where a saturated and weakened subsurface is loaded by the mass above it, though it remains unknown how this may increase the chances for future slope failure.

Such groundwater changes during glacier retreat have been found to be a critical element causing slope destabilization (Bovis and Stewart, 1998; Oestreicher et al., 2021). Grämiger et al. (2020) suggested that glacier changes at the toe of a landslide may resemble lake level fluctuations in the subsurface of the adjacent slopes. Changing lake levels, and particularly reservoir filling and drawdown cycles, have been shown to drive instability, as does the rate at which these cycles occur (Paronuzzi et al., 2013). The hydrological fluctuations driven by ice loss and the subsequent infilling of a proglacial water body, may mimic falling and rising lake levels and promote instability. Given that glacier mass loss is particularly rapid in southern Alaska (Hugonnet et al., 2021), the pace of these glacially driven subsurface hydrological changes is likely also relevant.

In addition to groundwater changes, there are mechanical changes when an ice buttress is replaced by water. Although ice can deform at very low strain rates (McColl et al., 2010) and has little influence on the slope stability (Storni et al., 2020), the buttressing provided by ice is more pronounced than the one provided by water after glacier retreat. Additionally, the rapid retreat rates of lake-terminating or tidewater glaciers mean that this change occurs relatively suddenly for landslides adjacent to deep water. As calving events occur and give way to the vertical cliffs that are characteristic of calving fronts (Cuffey and Paterson, 2010), slopes would experience drastic boundary changes in a short time frame. At Petermann Glacier, Greenland, for example, a single calving event in August 2010 led to the loss of around 250 km² of ice (Falkner et al., 2011). At Ilulissat (Jakobshavn) Glacier, Greenland, calving events in 2007 and ~~address the limitations of our methods. We also compare our results to previously published work and propose future research perspectives.~~ 2008 extended up to a kilometer horizontally and several hundred meters up-glacier (Amundson et al., 2008). The abrupt loss of large ice pieces may lead to localized structural changes within the landslide area (Grämiger et al., 2017; Hugentobler et al., 2022), which might cause additional, slope-scale redistribution of mechanical stress as the landslide mass starts to deform.

5.2 Landslide ~~activation-mechanisms~~interactions with the glacier and environment

Examining landslide and glacier evolution over several decades allowed us to determine the timing of what we refer to as landslide *activation*. It is possible ~~and indeed probable~~ that the underlying structures of these landslides have existed for many decades, centuries, or even millennia, and previous work has shown that landslides can reactivate or even fail millennia after deglaciation (Hermanns et al., 2017). We thus do not speak about landslide initiation, which would imply the motion onset, nor do we rule out that earlier phases of activity may have existed, ~~meaning that the displacements we observed are actually ones of a reactivation. Instead, we~~. We use the term *activation* to indicate the onset of detectable movement during our study period, while acknowledging that it may be a “reactivation” which we are observing.

When trying to establish a mechanism relating glacier ~~mass-loss~~changes to the observed instabilities, our sites can be divided into two categories: those where the glacier terminus has ~~already~~ retreated beyond the landslide and has been replaced by water, and those where the terminus is still downstream of the landslide. We will refer to landslides in the former ~~case and latter cases~~ as being impacted by “retreat-related” ~~debuitressing, and as and~~ “thinning-related” ~~debuitressing in the latter case, respectively~~. We acknowledge that glacier retreat and thinning are closely linked, meaning that the processes cannot be fully separated, but we use these terms to distinguish between slopes which have undergone a complete loss of glacier support from slopes in which some glacier buttressing is still present.

At Yale, Tyndall, Grand Plateau, and Barry, we observed a sudden activation of the landslides in response to rapid glacier retreat. In all four cases, the glaciers retreated past the landslides through lakes or fjords, and at rates up to ~~12~~seven times their long term average. ~~Marine and lake-terminating glaciers can retreat more rapidly in comparison to land-terminating glaciers due to feedback processes between ice dynamics and submarine topography. In particular~~For glaciers terminating in water, a combination of warm water intrusion (~~Weertman, 1974~~)(~~Weertman, 1974; Luckman et al., 2015~~), dynamic thinning (~~O’Neel et al., 2005; Benn et al., 2007~~), and surface melt ~~can cause the calving front to thin beyond the flotation level, thus causing rapid retreat though calving (Epprecht, 1987; Cuffey and Paterson, 2010)(Warren et al., 2001; Benn et al., 2007) may cause the terminus to thin to the point that it floats in a proglacial body of water (Warren et al., 2001). With part of the glacier floating, there is less basal friction and the glacier velocity can increase, thus supplying more ice to the calving front, and further thinning it (Benn et al., 2007)~~. Since the ~~calving rate is proportional to rate of calving tends to increase with~~ water depth, ~~the~~ retreat is fostered in ~~places with deeper water (Hanson and Hooke, 2000).~~

Such rapid, calving-driven retreat also means that at the corresponding locations, the landslide-ice interface is replaced with a landslide-water interface. The concomitant changes in water saturation of the landslide toe, together with structural changes induced by the redistribution of mechanical stresses as the landslide support changes from glacier ice to water, may partially explain the susceptibility of these slopes to sudden activation. Indeed, we hypothesize that such changes in boundary conditions are generally faster in the case of a rapidly retreating lake or marine-terminating glacier than they are at land-terminating glaciers, which may make a landslide activation more likely in the former case. Beyond this faster change, we believe there are several other relevant differences between this retreat-related situation and its thinning-related counterpart.

As a deeper water (Hanson and Hooke, 2000; Benn et al., 2007). These feedback processes between ice dynamics and submarine
670 topography cause the rapid retreat which is typical for marine- or lake-terminating glacier retreats past a landslide toe, the
forces acting upon the slope change significantly. In particular, the glacier provides buttressing support to the landslide prior to
glaciers.

In addition to the rapid retreat rate, there are other predisposing factors that may make these sites prone to acceleration.
First, three out of four sites are in sedimentary lithologies (Yale, Tyndall, and Barry), which are particularly susceptible to
675 water intrusion due to high porosity (Selley, 2005). Second, due to the maritime climate of southern Alaska and the low
elevation (Sec. 2), the glaciers at our study sites are presumably temperate, meaning that there is high water availability in
the subsurface prior to deglaciation. This combination of weakened and porous rock with high water availability may make
these landslides particularly likely to accelerate as the boundary conditions change during especially rapid glacier retreat.
Although ice can deform at very low strain rates (McColl and Davies, 2013), the buttressing is more pronounced than the one
680 provided by water after glacier retreat. This change occurs suddenly, owing to the vertical cliffs that are characteristic of calving
fronts (Cuffey and Paterson, 2010) and their fast retreat due to calving. This may lead to localized structural changes within
the landslide area, which might cause additional, slope-scale redistribution of mechanical stress as the landslide mass starts to
deform.

The other primary change relates to the hydrologic conditions at the landslide toe. Existing work indicates that during ice
685 sheet retreat, groundwater exfiltrates from the subsurface due to the decrease in ice overburden pressure while ice loading can
lead to ground compaction and the closing of fractures in the subsurface (Ravier and Buoneristiani, 2018). If the reverse were
true, i.e. if fractures open upon ice unloading, increased infiltration could occur after glacier retreat. This would in turn lead to
increased pore water pressure, which was found to be positively correlated to landslide movement (McColl, 2015). Regardless
of the direction of the subsurface fluxes, hydraulic gradients caused by groundwater fluctuations can impact slope stability
690 (McColl, 2015), and the change from a landslide in contact with ice to a landslide in contact with water will undoubtedly alter
these gradients.

For landslides near the termini of marine-terminating glaciers, tidal forces may also play a role in the destabilization. Prior to
complete glacier debuttressing, the glacier ice would largely protect the landslide from both tides and waves. Once the glacier
has retreated, the slope would become vulnerable to both cyclical tidal forces and wave action. Together, these processes may
695 cause increased erosion and rearrangement of sediment, which can in turn impact landslide stability (Doi et al., 2020). The
increased erosion might also reinforce itself, as the released materials can further increase abrasion (Payo et al., 2016), thus
further affecting the overall landslide stability.

The above considerations suggest that landslides adjacent to rapidly retreating lake- or marine-terminating glaciers may be
particularly susceptible to ~~activation~~destabilization. However, ~~various forms of landslide activity were~~ landslide activity was
700 also detected for sites that “only” experienced thinning. At both Ellsworth and Alsek, for example, landslide activation occurred
6 to 8 years after glacier thinning increased by a factor of ~ 2 . Lacroix et al. (2022) made a similar observation ~~for in~~ Iceland,
where a landslide acceleration ~~at Tungnakvíslarjökull~~ followed 6 years after a marked increase in glacier thinning rate. ~~One~~
~~hypothesis is~~ Kos et al. (2016) proposed that landslide activation ~~begins may begin~~ after the glacier ice thins to a critical thick-

ness. For the Moosfluh landslide in Switzerland, for example, Storni et al. (2020) found that slope displacements were ~~higher~~
705 ~~larger~~ where ice thickness was below 50 m and smaller where the ice was ca. 100 m thick, while Glueer et al. (2019) found
that the whole landslide accelerated after the ice ~~thickness~~ thinned below 100 m. Our results ~~instead~~ show that the landslide
accelerations at Ellsworth and Alsek occurred when the local ice thickness was ~~still in on~~ the order of 300 m (Ellsworth) to
350 m (Alsek), ~~indicating that such thickness thresholds are site specific. However, these numbers cannot be directly compared~~
~~to the Moosfluh case, which is an alpine glacier in very different climatic conditions, but may imply region-specific thinning~~
710 ~~thresholds~~. Taken together, thinning-related debuttreasing does not seem sufficient to explain all of the observed landslide be-
havior, and indeed, the Portage landslide deformed continuously as the glacier thinned ~~while no acceleration was seen, and no~~
~~evident acceleration was detected~~ at Columbia despite an increase in glacier thinning rate by ~~almost~~ a factor of ~~three~~.

Precipitation might be a further cause of landslide activation, in addition to glacier changes. ~~In one case (Ellsworth, cf. Sect. 4.3.1), Here, we chose to investigate temporal resolutions that are consistent with the available information on glacier~~
715 ~~and landslide changes, acknowledging that by doing so we cannot capture the full variability of the meteorological processes.~~
~~Existing literature shows that landslides can respond to a wide range of precipitation totals, both in wet and dry climates~~
~~(Handwerger et al., 2022), and on timescales ranging from minutes to several months (Iverson, 2000; McColl, 2015). Similarly,~~
~~there is evidence that interannual precipitation changes play a role, with a number of landslides being initiated during rainy~~
~~years following a drought (Handwerger et al., 2019a). Lacroix et al. (2020) states that elevated landslide velocities are typically~~
720 ~~seen during i) periods with intense precipitation, ii) times with long-lasting precipitation, or iii) the melt season, but that~~
~~landslide response to precipitation also depends on the local geology, the specific characteristics of the instability, as well as~~
~~the local topography and hydrology.~~

In the case of Ellsworth, we found above-average July precipitation coinciding to landslide acceleration, although the pre-
cipitation total in July was lower than typical autumn amounts. This indicates that the total precipitation was not unusual for
725 the site, while the timing was. This could be relevant for two reasons. First, the available temperature data indicate that the
precipitation likely fell as rain in July ~~and as~~, as opposed to snow in autumn (Fig. ??G1 in App. G). Second, the subsurface
may have been additionally saturated from ice melt in summer. Together, these conditions could have led to above-average
pore water pressure and thus, to the observed landslide acceleration. Being based on observations of one site only, however,
we recognize ~~the that~~ such a mechanism remains speculative.

730 Also the relation between seismic activity and landslide activation remains inconclusive. Our study period began in 1980,
16 years after a magnitude 9.2 earthquake rocked Alaska (Kanamori, 1977), and it is not excluded that such a large seis-
mic event might have weakened the various slopes through mechanical damage without causing instantaneous failure. ~~In an~~
~~analysis focusing on central Italy, for example, Song et al. (2022) found that landslide accelerations occurred in areas with~~
~~light-to-moderate ground-shaking.~~ This is in line with findings by McColl (2015), who noted that i) landslides can withstand
735 many dynamic events (such as due to seismic activity) without failing and ii) the event triggering catastrophic failure may
not be the largest. In an analysis focusing on central Italy, for example, Song et al. (2022) found that landslide accelerations
occurred in areas with light-to-moderate ground-shaking. While we do not find a direct link between seismic activity and

slope accelerations in our data, we ~~still suggest~~ recognize that seismic events can contribute to the development of instabilities through a preconditioning of the related slopes.

740 5.3 ~~Evolution following landslide activation~~

~~Our results show that~~ There are additional factors which, while relevant for slope stability, did not play a central role in this analysis. For example, the site-specific structural geology, such as the composition of the landslide and the fracturing of the subsurface, is undoubtedly a critical factor for slope stability. The subsurface properties cannot be determined without intensive field studies, but such studies are not feasible at the scale studied here. Similarly, we did not consider any specific information
745 ~~on the slopes' hydrology, as such information is simply not available. Plus, it is closely linked to subsurface fracturing, which cannot be determined from remote sensing. Slope hydrology is also influenced by seasonal melt events. Annual snowpack releases large amounts of water into the slope, which may impact stability. Detailed analyses on snow hydrology are outside the scope of this work, but an analysis of total solid precipitation over the time period 1980–2022 did not show a correlation with landslide activation (Fig. G3 in App. G).~~

750 ~~Our results suggest that paraglacial landslides—especially those that are in contact with a lake or fjord after glacier retreat—may respond rapidly to glacier mass loss. However, the initial landslide response to~~ ~~glacier retreat~~ does not determine the long-term evolution of the landslide. ~~In particular, both, where both a~~ re-stabilization ~~and/or~~ catastrophic failure might occur. At Yale, for example, no further large-scale movement followed after the landslide activation in the early 1990s. ~~This is different from what was observed~~ ~~On the other hand,~~ at Barry and Grand Plateau, ~~where~~ measurable deformation continued after activation. Barry
755 accelerated rapidly and then slowed, while Grand Plateau moved at a constant, accelerated pace. ~~Tyndall, instead, is an example for a landslide that evolved to catastrophic failure. While slow movement may continue for a long period of time, landslides can experience periods of acceleration and some even progress to catastrophic failure (Lacroix et al., 2020), with Tyndall being an example of the latter. The reason why some landslides maintain a slow velocity and others speed up or fail is unknown, but slow motion is typically observed prior to failure (Hendron and Patton, 1987; Handwerger et al., 2019b; Federico et al., 2011). This transition from slow to fast movement may be related to decreasing porosity in the shear-zone (Agliardi et al., 2020; Iverson et al., 2000), decreasing viscosity of the landslide material (Mainsant et al., 2012; Carrière et al., 2018), or shear localization (Voight, 1988; Lacroix and~~
760 ~~and is a topic of ongoing research.~~

~~Once the glacier retreats past the landslide, it can no longer be the factor controlling landslide displacements. Hydro-geologic mechanisms must become dominant. An example of these changing controls is the situation at Barry, where a head scarp~~
765 ~~was already visible in 1957 imagery of the U.S. Air Force, indicating that the landslide was active prior to the acceleration in the early 2000s. We do not know how long the head scarp persisted, nor what caused its original formation. However, our analyses and the findings of Dai et al. (2020) suggest that glacier retreat was an important mechanism as the terminus passed the landslide toe. The idea that the controlling mechanism can change over time (see also Schaefer et al., 2023, for the Barry case) ; means that periodic assessments are necessary to understand and address the evolving hazard.~~

770 ~~In cases where the terminus has not yet retreated past the landslide, the question remains about what will happen when that occurs. One hypothesis is that the landslides will reach a new equilibrium as the glaciers thin and the slopes (re-)adjust to the~~

changed boundary conditions. Another hypothesis is that thinning-related debuttreasing will cause critical weakening of the slopes, eventually leading to landslide acceleration. While our results let us favor the latter hypothesis, it remains unknown if such accelerations will eventually also increase the chances for future slope failure.

775 5.3 Methodological limitations

In this work, we relied on ITS-LIVE as one source of landslide displacement velocities. The dataset was originally designed for quantifying glacier flow velocities, so the processing parameters are optimized for velocities that are much higher than for typical landslide motion. The coarse resolution of the dataset also means that small displacements cannot be detected accurately. ITS-LIVE is thus expected to perform better for larger and fast-moving landslides, where surface features and
780 resulting displacements are larger. The same is true for displacements measured by manual feature tracking, where we expect that the minimum measurable displacement is around two pixels, i.e. 60 m. Small changes or displacements of landslide are by no means irrelevant, but the resolution provided by both the feature tracking datasets seem adequate for investigating the slope-wide responses of the landslides to glacier changes.

In some areas, the ITS-LIVE data also appears to show some “leakage” of the glacier signal to glacier-adjacent pixels. This is especially apparent at Portage Glacier, where several pixels classified as non-glacier have very high velocities and move
785 parallel to the glacier (Fig. 3). This may result from i) uncertainties in the glacier margins, ii) temporal inconsistencies between the glacier margins and the ITS-LIVE data, or iii) a large window size used during the process of image cross-correlation. This leaked signal typically extends 1 to 2 pixels (i.e. up to 240 m) away from the glacier and thus affects a small portion of the landslides’ extents. We do not expect this leakage to impact our results, however, as we only compute velocities within a
790 defined “active area” (see Sect. 3.1). The confidence in the methods used here is further increased by the good agreement between ITS-LIVE derived displacements and existing work at Barry Glacier (see Sect. 5).

To determine the importance of the glacier changes, we also analyzed time series of precipitation. However, determining an appropriate time scale for such an analysis is challenging, as landslides can be activated by both heavy precipitation events of short duration as well as extended periods of particularly wet conditions. Indeed, existing literature shows that
795 landslides can respond to a wide range of precipitation totals, both in wet and dry climates (Handwerger et al., 2022), and on timescales ranging from minutes to several months (Iverson, 2000; McColl, 2015). Similarly, there is evidence for the interannual precipitation changes to play a role, with a number of landslides being initiated during a rainy year following a drought (?). The landslide response to precipitation also depends on the local geology, the specific characteristics of the instability, as well as the local topography and hydrology (Lacroix et al., 2020). Lacroix et al. (2020) states that elevated landslide
800 velocities are typically seen during i) periods with intense precipitation, ii) times with long-lasting precipitation, or iii) the melt season. For our analysis, we chose to investigate temporal resolutions that are consistent with the available information on glacier and landslide changes, acknowledging that by doing so we cannot capture the full variability of the meteorological processes.

There are several additional factors which we did not consider in this work. For example, the site-specific structural geology, such as the composition of the landslide and the fracturing of the subsurface, is undoubtedly a critical factor for slope stability.
805

~~The subsurface properties cannot be determined without intensive field studies, but such studies are not feasible at the regional scale studied here. Similarly, we did not consider any specific information on the slopes' hydrology, as such information is simply not available. Lastly, we did not explicitly consider snow heights, as we expect this factor to be correlated with precipitation.~~

810 5.3 Comparison to previous works

~~Existing~~ Other work at five of the eight sites has independently confirmed landslide movement. Schaefer et al. (2024) found average line-of-sight speeds ranging from 0.41 to 9.64 mm.yr⁻¹ for Ellsworth, Portage, Barry, Yale, and Columbia. These values are very different from the ones obtained in this work, which we attribute to the differing methods ~~used, as well as~~ and different periods of investigation. While Schaefer et al. (2024) used InSAR data, which measures small displacements but may
815 not be suitable for large accelerations (Manconi, 2021), we employed lower resolution satellite data. Additionally, Schaefer et al. (2024) investigated the period 2016-2022, and we characterized the long-term ~~landslide~~ evolution over a 40-year period. Of the 43 sites investigated by Schaefer et al. (2024), 11 were ~~assessed as having the potential to generate a tsunami~~ determined to be potentially tsunamigenic, and four of those 11 sites are also studied here. Regardless of the drivers, landslide movement and accelerations ~~observed~~ near deep lakes or fjords have important hazard implications.

820 In-situ measurements at Portage and Columbia have also confirmed movement at those sites. Deformation up to 5 m at the Portage landslide is visible in high-resolution digital image correlation between 2022 and 2023 (Lemaire et al., 2023b). This is ~~somewhat~~ higher than the ~~2.12 m.yr⁻¹~~ 2.1 m.yr⁻¹ detected by ITS-LIVE on average over ~~2021-2022~~ 2021-2022 (Fig. 4fHf). At Columbia, movement on the order of ~~several a few~~ centimeters per year has been detected using GPS (~~B. Higman, personal communication~~) (Jeffries, 2023) and InSAR (~~M. Jacquemart, personal communication~~ see Supplementary Materials).
825 The discrepancy between these numbers and our results can ~~easily~~ be explained by the resolution of the satellite imagery (see Sect. ~~??3.1~~).

At Barry, Dai et al. (2020) characterized the landslide movement since 2000 using feature tracking. A comparison to ~~our~~ the ITS-LIVE results shows generally good agreement in terms of both timing ~~of acceleration~~ and average velocity magnitudes, the largest differences being found in the period 1999-2008, when the uncertainty is ~~also~~ largest, and the smallest differences
830 being found in the periods 2010-2013 and 2014-2016 (~~Table-Tab.~~ 1). In their analysis, Dai et al. (2020) used imagery from Landsat (as we did), but also from ASTER, WorldView-1, and Ikonos, which have partly much higher resolution. This may explain some of the discrepancies.

5.4 Future research perspectives

Our study suggests that the rapid retreat of lake- and ~~marine-terminating~~ marine-terminating glaciers can lead to the sudden
835 activation of paraglacial landslides near bodies of water. Since the retreat rate in such cases is related to water depth (~~as deeper waters imply enhanced calving~~ Sect. 5.2), this raises the question whether landslide activation is preferentially co-located with deeper-than-average sections of lakes or fjords. Accurate bathymetric data would help ~~answering~~ answer this question, as they provide a detailed picture of the submarine environment adjacent to the landslides. If such a relation between water depth and

Table 1. Comparison of landslide velocity at Barry Glacier from Dai et al. (2020) and this work. The ‘Ratio’ is computed by dividing the value from this work by the value from Dai et al. (2020).

Time Period	Dai et al. (2020) [m yr ⁻¹]	This Work [m yr ⁻¹]	Ratio [-]
1999 - 2008	1.3 ± 0.6	6.4 ± 4.8	4.9
2010 - 2013	26 26.2 ± 3 3.0	22.2 ± 6.0	0.9 0.8
2014 - 2016	10 9.6 ± 2 2.0	11.3 ± 1.7	1.1 1.2
2017 - 2020	1.3 ± 1.7 0.7	1.7 ± 0.2	1.3

landslide activation exists, ice thickness datasets ~~as used in this work~~ (Farinotti et al., 2019; Millan et al., 2022) could be used
840 to estimate the up-valley extent of the lakes or fjords and thus potential future water depths. This would be informative from a hazards perspective, also because the velocity of a potential tsunami triggered by a landslide collapsing into water is known to be proportional to water depth (Okal, 1988).

In terms of mechanistic understanding of the processes at play during landslide activation, the four cases where rapid glacier retreat coincided with landslide activation are obviously not sufficient to establish conclusive causalities. Broader regional
845 studies with a focus on paraglacial landslides adjacent to lake- or marine-terminating glaciers would be helpful in this respect. At a more local level, detailed observations at sites where the glacier terminus is projected to soon pass the landslide area (e.g. Portage and Columbia) could yield valuable insights into the changing boundary conditions. Together, such regional and local studies could also help in further testing our framework distinguishing retreat- versus thinning- dominated debuttreassing.

As glaciers continue to retreat and expose new fjords and lakes, the proximity of instabilities to water will change. This
850 will have consequences in terms of hazard disposition and possible mitigation measures. We argue that additional observations would be useful in order to monitor known landslides and detect newly forming instabilities in a timely manner. Together, this may help to minimize the risk that a rapidly evolving environment poses to the public.

6 Conclusions

This work provides a ~~regional overview of~~ comparison of several glacier debuttreassing-related instabilities in southern coastal
855 Alaska. We ~~selected~~ studied eight large landslides which are currently in contact with a glacier or have been so in recent decades, and which show signs of recent activity. At all sites, we use feature tracking in combination with glaciological, meteorological, and seismological datasets to examine correlations between slope movement and environmental changes between the 1980s and present-day. To extract slope velocities, we primarily use the ITS-LIVE dataset. While this dataset has fairly coarse resolution (120 m) and was originally designed for quantifying glacier flow velocities, comparison with in-situ
860 observations (Dai et al., 2020) attest the suitability of the dataset for our purposes ~~-(Sec. 5.3).~~

We find that ~~the~~ six out of the eight sites underwent significant slope acceleration at some stage during the studied time period. At four sites, such an acceleration occurred as the glacier terminus retreated past the landslide area. In these cases, the

landslides border deep water bodies and we suggest that they underwent rapid debuttreasing as the glacier retreated up-valley. For another two sites, landslide acceleration either coincided with a particularly rainy month, or with a significant increase in glacier thinning. The remaining two sites instead showed either slow, constant movement without a specific period of acceleration, or no detectable movement at all. In terms of causality, we ~~hypothesize~~ suggest that the landslide accelerations were related to a loss of mechanical support from the glacier and ~~to~~ changes in the landslide hydrology. ~~For the marine-terminating cases, we furthermore suspect that tidal forces eroding the landslide toe may have played a role.~~

The presence of large, unstable slopes poses a significant hazard, particularly when located in the vicinity of deep water. The rapid ongoing glacier retreat could expose more such slopes in the future, potentially increasing the risk for some of these to fail catastrophically. In this context, we see two potential avenues for further work: First, more detailed investigation of the sites would be enlightening, since only limited information can be gained from ~~a regional perspective~~ remote sensing methods. In-situ monitoring, for example, would provide more reliable data than available via the ITS-LIVE results, as well as a more complete picture of the local processes. This is particularly important at sites that will experience debuttreasing in coming decades, such as Portage or Columbia. Second, we see potential in using the ITS-LIVE data for detecting landslide events at ~~the~~ a larger, potentially worldwide, scale. Some aspects, such as the detection limits of the method and the leakage of the glacier signal to neighboring areas, would need to be addressed for that, but could lead to the early detection and monitoring of landslides at the regional scale. ~~On~~ Such a regional overview would allow for correlating landslide activity with various factors over a broader area, specifically elevation, aspect, precipitation amount, and proximity to faults, to name a few. In the longer term, such a development could assist in dealing with the hazards that stem from a rapidly changing environment.

Code and data availability. Please contact the first author regarding the availability of code and data used in this work.

Video supplement. Videos showing the landslide activation at four sites are available as supplementary material.

Appendix A: Site Description

A1 Ellsworth

885 Ellsworth Glacier is a lake-terminating glacier located on the Kenai Peninsula, around 30 km east of Seward, Alaska (Fig. 1B and Fig. 2). It is oriented to the southwest and flows from a glacier complex at over 1800 m a.s.l. to nearly sea level (10 m a.s.l.). There are a series of instabilities along the western edge of the glacier, where the glacier bends. We focus on the instability which is largest and farthest up-glacier, spanning a distance between 2.5 and 4 km from the 2021 terminus. The instability is characterized by a prominent main scarp and an active talus source area (Higman et al., 2023). Movement
890 at the site between 2016 and 2022 has been confirmed by Schaefer et al. (2024) using interferometric synthetic aperture radar (InSAR). The instability is located in sedimentary rocks of the Orca group (Eocene to Paleocene age) and the lithology of the group is sedimentary, consisting primarily of sandstone and siltstone (Wilson et al., 2015). The volume is estimated between 66 and 150 Mio. m³ (14 to 113 Mio. m³ according to Schaefer et al. (2024); Tab. D2 and App. D).

A2 Portage

895 Portage Glacier is a lake-terminating glacier located at the northern part of the Kenai Peninsula, around 7.5 km southwest of Whittier, Alaska (Fig. 1A and Fig. 2). The glacier flows northeast and extends from an ice field at 1430 m a.s.l. to around 60 m a.s.l.. At the north end of the glacier, where the glacier calves into Portage Lake, there are two instabilities. We focus on the larger and more active of the two, laying farther up-glacier, between 200 and 1100 m from the 2021 terminus. The instability shows clear signs of deformation including tension cracks, a main scarp, a talus source area, and antiscarps (Higman et al., 2023)
900 . Rockfall activity has been observed at the site and surficial streams on the slide disappear into the subsurface (Higman et al., 2023). InSAR data suggest the landslide moved between 2016 and 2022 (Schaefer et al., 2024). The instability is located in Chugach flysch (Upper Cretaceous age) and the lithology is sedimentary, composed primarily of metagraywacke and metasiltstone (Wilson et al., 2015). The instability has a volume of around 11 to 35 Mio. m³ (5 to 19 Mio. m³ according to Schaefer et al. (2024); Tab. D2 and App. D).

905 A3 Barry

Barry Glacier is a tidewater glacier flowing southwest into Barry Arm in Prince William Sound, around 50 km northeast of Whittier, Alaska (Fig. 1A and Fig. 2). The glacier flows from an accumulation area in a large ice complex in the Chugach Mountains at 2700 m a.s.l. to sea level. The region around the glacier terminus is very dynamic. There are a number of instabilities to the northwest and southeast of the terminus. We focus on the largest instability, which is characterized by anti-
910 and normal-scarps, a main scarp, and a talus slope area (Higman et al., 2023). Multiple studies have confirmed the movement of this landslide since 2000 (Dai et al., 2020; Schaefer et al., 2024). Like Portage, the Barry instability is located in Chugach flysch. As of 2021, around half of the landslide toe was buttressed by the glacier, though the glacier has been retreating past the

instability since 2010. The Barry instability is the second largest in this study, with an estimated volume of 188 to 500 Mio. m³ (117 to 564 Mio. m³ according to Schaefer et al. (2024); Tab. D2 and App. D).

915 A4 Yale

Yale Glacier is a tidewater glacier terminating in College Fiord in Prince William Sound, approximately 70 km northwest of Valdez, Alaska (Fig. 1A and Fig. 2). It flows from a large glacier complex in the Chugach Mountains at around 3600 m a.s.l. to sea level. Within 2 km of the present-day terminus, there are three instabilities. We focus on the largest of the three, which has a volume between 255 and 750 Mio. m³ (145 to 1025 Mio. m³ according to Schaefer et al. (2024); Tab. D2 and App. D). The
920 instability is characterized by anti- and normal-scarps, a talus slope area, shear zones, and tension cracks (Higman et al., 2023), and movement of the landslide has been confirmed with InSAR (Schaefer et al., 2024). As with the other nearby instabilities, the lithology of this site is Chugach flysch. The landslide started to become ice-free around 1977, but it took until 2021 for the terminus to completely retreat past the toe area.

A5 Columbia

925 Columbia Glacier, located around 35 km northwest of Valdez, Alaska (Fig. 1A and Fig. 2), is likely one of the most well-known glaciers worldwide due to its striking retreat over the past decades. The highest reaches of the glacier are nearly 3700 m a.s.l. in the Chugach Mountains and it flows to the south down to sea level in Prince William Sound. Near the present-day terminus of Columbia Glacier, there are several instabilities to the north. We select the instability which is closest to the terminus (between 500 and 1800 m in 2021) and which could pose the largest hazard in the coming decades. The instability is characterized by
930 tension cracks, normal scarps, a talus slope, and a lake which drains periodically (Higman et al., 2023). InSAR results from Schaefer et al. (2024) suggest the landslide moved between 2016-2022. The lithology of the instability is Chugach flysch. It has a volume of approximately 44 to 150 Mio. m³ (17 to 111 Mio. m³ according to Schaefer et al. (2024); Tab. D2 and App. D).

A6 Tyndall

935 Tyndall Glacier is located in the St. Elias mountain range and terminates at sea level in Taan Fiord, around 110 km northwest of Cordova, Alaska (Fig. 1C and Fig. 2). The glacier is bordered by some of Alaska's tallest mountains, with an accumulation area reaching up to 5290 m a.s.l.. There are a number of instabilities near the terminus of Tyndall Glacier. We select the one that failed catastrophically in 2015, which had a volume of 63 Mio. m³ and caused a tsunami with 193 m runup (Higman et al., 2018). The remaining sliding mass is around 100 Mio. m³ (Tab. D2 and App. D). This site is thus distinct from the others because it
940 has already experienced a catastrophic failure. The instability at Tyndall is located in the Kulthieth Formation, a sedimentary lithology from the Eocene composed of conglomerate-mudstone (Wilson et al., 2015). As of 2021, the glacier buttresses the length of the landslide toe. After a rapid retreat in the late 1980s, the glacier terminus was up-valley with respect to the landslide but has been stable or slowly advancing since the early 1990s.

A7 Alsek

945 Alsek Glacier is located in southeastern Alaska, around 100 km from Yakutat (Fig. 1D and Fig. 2). Alsek Glacier flows from an elevation of 2420 m.a.s.l. down to 60 m.a.s.l.. The glacier terminates in Alsek Lake, which has grown from a few square kilometers in the 1950s to about 75 km² today as the glacier has retreated (Loso et al., 2021). Between 3.5 and 5 km up-glacier from the 2021 terminus, an instability with a volume between 19 and 50 Mio. m³ (Tab. D2 and App. D) is found on the eastern side of a nunatak. The failure is characterized by a large head scarp which extends around 1 km laterally. The instability
950 at Alsek Glacier is found in volcanic rocks of the Chugach accretionary complex, a metamorphic lithology from the Upper Cretaceous (Wilson et al., 2015). Gneiss, migmatite, and schist are the primary rock types (Wilson et al., 2015).

A8 Grand Plateau

Grand Plateau Glacier is located in southeast Alaska, around 120 km from Yakutat (Fig. 1D and Fig. 2). It is a very large glacier, spreading over an area of 237 km² and spanning an elevation range of nearly 4600 m. The glacier currently terminates
955 in three different lakes. We focus on the southeastern branch, where an instability with a volume of 50 to 150 Mio. m³ is present (Tab. D2 and App. D). The instability at Grand Plateau Glacier is located on an east-facing mountainside at the glacier left. The terminus began retreating past the instability around 2010, and the instability was completely debuttressed in 2022. It displays signs of movement through scarps, and like Alsek, it is located in volcanic rocks of Chugach accretionary complex.

Appendix B: DEM ~~Years~~years

Table B1. Summary of the years for which a DEM is available at the sites of interest. “BER” and “DEH” refer to the DEMs of Berthier et al. (2010) and Dehecq et al. (2020), respectively. Note that for the Dehecq et al. (2020) DEMs, multiple elevation models within a year may have been merged to generate the final product.

Name	Year (BER)	Year (DEH)	Notes (BER)
Ellsworth	1950	-	
Portage	1950	1980	
Barry	1957	1979-80	
Yale	1957	1979-80	
Columbia	1957	1979	
Tyndall	1972	1977	very small portions in the accumulation area are from 1974 or 1976
Alsek	1948	1977-78	
Grand Plateau	1948	1977-78	a portion of the accumulation area is from 1987

960 Appendix C: Glacier characteristics

Glaciological characteristics of each site. “ $\Delta H_{gl,X}$ ” is the median elevation change of the glacier within the instability-adjacent glacier polygon (see Sect. C and Fig. 2 for definition), where X is either 1 for the period 1960–1978, 2 for 1978–2000, or 3 for 2000–2020. Note that i) the values for $\Delta H_{gl,1-2}$ for Ellsworth and Columbia refer to the period 1960–2000, and ii) the values for $\Delta H_{gl,3}$ are an average of the 2000–2005, 2005–2010, 2010–2015, and 2015–2020 changes. “ $H_{gl,F}$ ” and “ $H_{gl,M}$ ” are the median thicknesses of the glacier within the instability-adjacent glacier polygon from Farinotti et al. (2019) and Millan et al. (2022), respectively. $\Delta H_{gl,1}$ $\mathbf{m\ a^{-1}}$ -2.7 1.25 -5.61 -3.29 -1.33 -1.97
 $\Delta H_{gl,2}$ $\mathbf{m\ a^{-1}}$ -1.7 0.48 -5.42 -9.55 -1.81 -3.3
 $\Delta H_{gl,3}$ $\mathbf{m\ a^{-1}}$ -2.51 -1.62 -9.65 -2.18 -14.1 0.56 -2.85 -5.85
 $H_{gl,F}$ \mathbf{m} 220 170 230 210 660 120 260 480
970 $H_{gl,M}$ \mathbf{m} 250 200 280 260 400 240 280 260

Appendix C: Monthly meteorological data

Average monthly precipitation at all sites which experienced a landslide acceleration during the study period. Thicker, darker blue lines correspond to the year or years during which the landslide accelerated, while light blue lines are all other years. The solid gray line corresponds to the mean monthly precipitation over the whole time period (1979–2022), and the gray dashed lines are two standard deviations above and below the mean. Note the differing y-axes of the various subplots. All x-axes refer to the labels on the bottom row.

Average monthly temperature at all sites which experienced a landslide acceleration during the study period. Thicker, darker red lines correspond to the year or years during which the landslide accelerated, while light red lines are all other years. The solid gray line corresponds to the mean monthly temperature over the whole time period (1979–2022), and the gray dashed lines are two standard deviations above and below the mean. The black dashed line marks zero degrees Celsius. Note the differing y-axes of the various subplots. All x-axes refer to the labels on the bottom row.

Appendix C: Feature definition

Instability-adjacent-glacier polygon

We created an instability-adjacent-glacier polygon to examine the glacier changes near the instability. For sites where the instability is far from the current terminus, we created a glacier polygon that is the same width as the instability. For sites where the instability is currently near the terminus, we manually created a polygon around 1 km long starting from the smallest extent and then intersected this with the glacier outlines from RGI Consortium (2017). Note that the smallest extent of the glacier is not necessary at present-day.

Cross section

990 We generated cross sections through the landslide and glacier to study the glacier elevation changes near the instability. A line was drawn between the centroid of the instability polygon and the closest point on the centerline. Using the QGIS function “Extend lines,” the line was extended by 4000 m in each direction. Points were then generated on the cross section at 10 m intervals using the QGIS function “Points along geometry.” For these points, we then extracted values for each of the four available DEMs. For the cross section, we considered the area between the ridgetop behind the instability and the thickest part
995 of the glacier.

Appendix D: Landslide volume

In order to determine landslide volume, it was first necessary to determine the landslide extent. We delineated a polygon from high-resolution imagery or lidar by selecting all topographic features that showed signs of deformation. [Subglacial and submarine extents were estimated using bedrock topography determined from the datasets mentioned in Section 3.4.1.](#) Then, landslide volume was determined in two different ways: empirically and by expert estimation. We used an empirical relationship between the landslide surface area A_S and its volume V of the form

$$V = k \cdot A_S^\beta,$$
 (D1)

where k and β are two empirical coefficients. We used three different sets of coefficients corresponding to a worldwide average for landslides, a worldwide average excluding shallow and submarine landslides, and an average for large landslides (Tab. D1). In addition, we completed expert estimation using the instability polygon and by inferring a sliding surface. To do so, the angle of the head scarp was extrapolated into the subsurface where available, and a concave failure plane was assumed in each case. We then estimated the volume between the basal failure plane and the surface.

Table D1. Different β and k coefficients used for estimating the volume of the instabilities V based on the instabilities’ surface area A_S (Eqn. D1). “Number” is a key for the method in Table D2.

Number	Source	β	k	Note
1	Guzzetti et al. (2009)	1.450	0.074	worldwide study
2	Jaboyedoff et al. (2020)	1.362	0.288	similar to (1) without shallow or submarine landslides
3	Jaboyedoff et al. (2020)	1.375	0.410	mean of range for large landslides

Table D2. Geological characteristics of each site. “ $V_{ls,X}$ ” are the estimated volumes of the instability, where X is either E for the volume determined using expert opinion, 1-3 using the empirical methods from Table D1, or S referring to the average of the volumes given by Schaefer et al. (2024). For Tyndall, the value in parentheses is the volume remaining at present-day. “ A_{ls} ” is the area of the instability from the delineated outline.

	Ellsworth	Portage	Barry	Yale	Columbia	Tyndall	Alsek	Grand Plateau
$V_{ls,E}$ [Mm ³]	150	35	500	750	150	160 (100)	50	150
$V_{ls,1}$ [Mm ³]	66	11	188	255	44	62	19	50
$V_{ls,2}$ [Mm ³]	74	14	196	262	50	69	23	57
$V_{ls,3}$ [Mm ³]	127	24	339	454	86	118	39	98
$V_{ls,S}$ [Mm ³]	14-113	5-19	117-564	145-1025	17-111	-	-	-
A_{ls} [km ²]	1.5	0.4	3.1	3.8	1.1	1.4	0.6	1.2

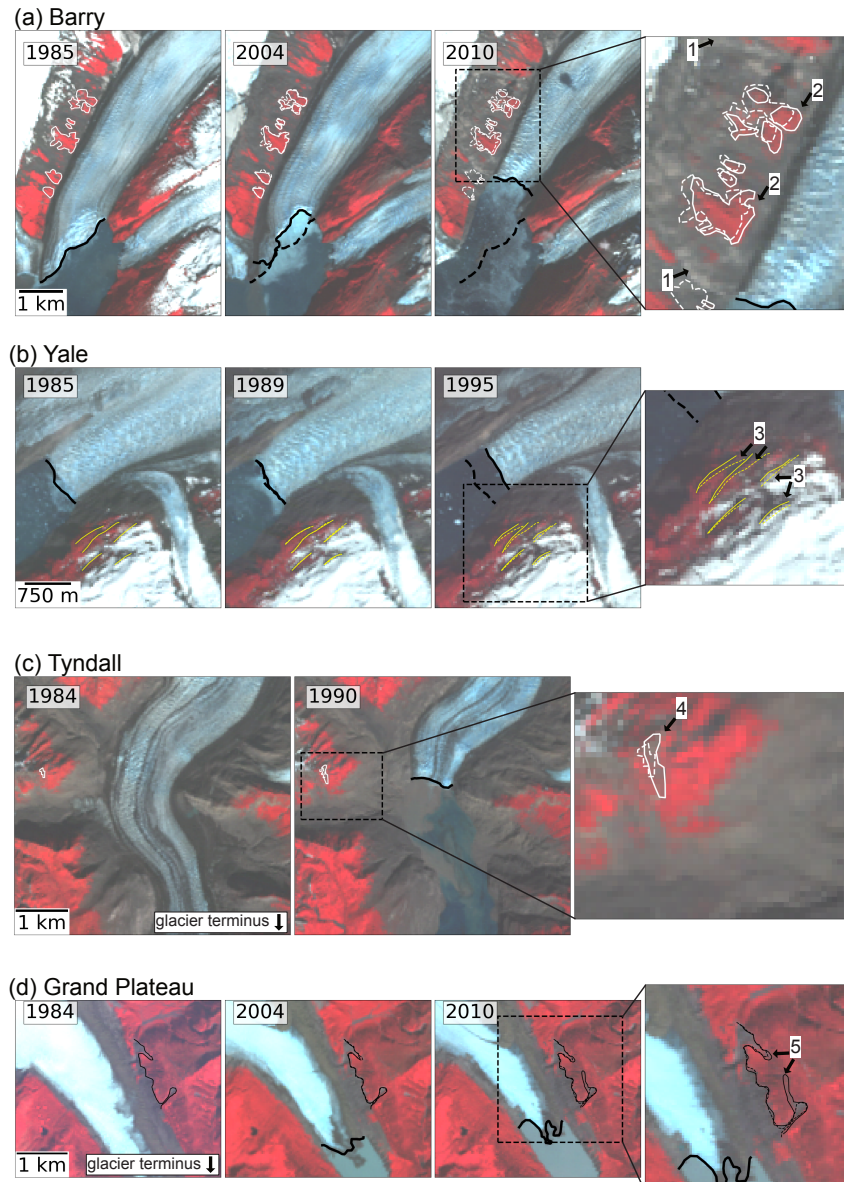


Figure E1. Landslide features and glacier terminus position during movement onset for sites where the terminus has passed the landslide. The year of acquisition of the individual satellite images is given at upper left. The panel at far right shows a zoomed version of the previous panel (shown by the black dashed box). Solid lines refer to the year at upper left in each image and for subsequent years, dashed outlines refer to the first time period (image at far left). Arrows highlight the formation of a head scarp (1), downward displacement of vegetation patches (2), downward displacement of surface features (3), widening of a crack (4), and the formation of a crack (5). Panels A-D refer to Barry, Yale, Tyndall, and Grand Plateau, respectively. Background images are Landsat 4-7 courtesy of the U.S. Geological Survey.

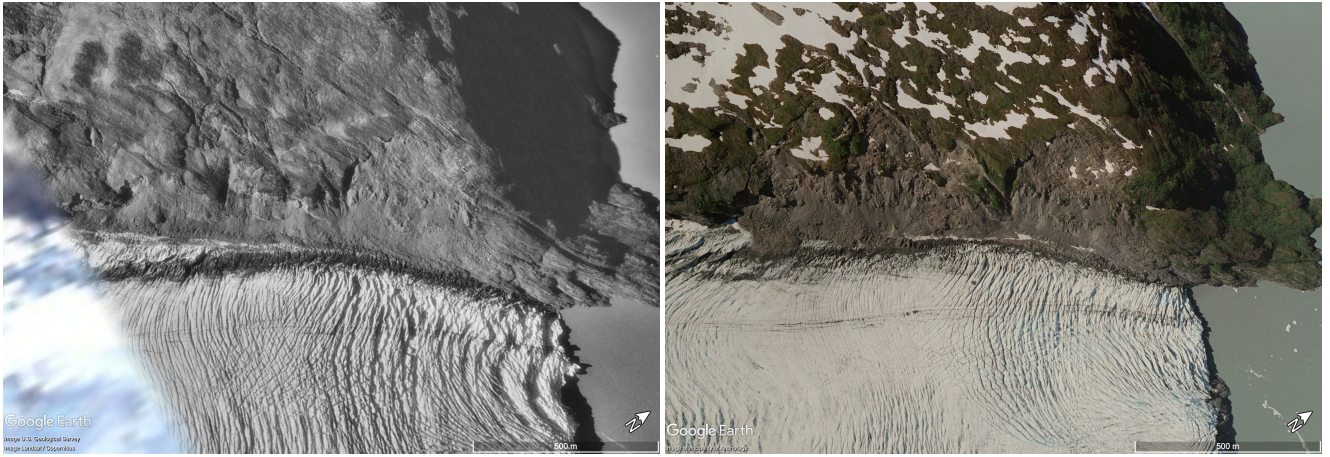


Figure E2. Images of Portage Glacier landslides in 1996 (left) and 2006 (right) show the evolution of the landslide throughout time and the disintegration of the slope. A scale bar and north arrow are at lower right. Both images are from Google Earth (Google Earth Pro, a, b).

Appendix F: Glacier characteristics

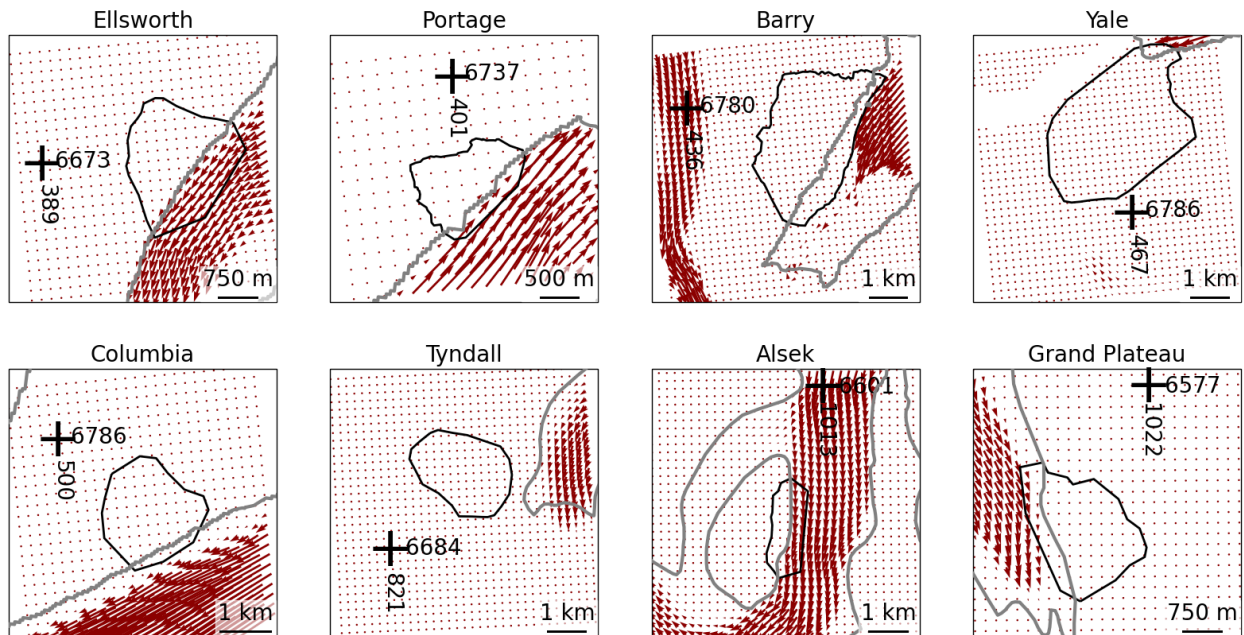


Figure F1. Average (1984-2022) displacement vectors from ITS-LIVE data. Glaciers are marked by gray (outlines from RGI Consortium (2017)) and black outlines mark the instability polygon. Coordinate crosses are given in UTM 6.

Table F1. Glaciological characteristics of each site. “ $\Delta H_{gl,X}$ ” is the median elevation change of the glacier within the instability-adjacent glacier polygon (see App. C and Fig. 2 for definition), where X is either 1 for the period 1960-1978, 2 for 1978-2000, or 3 for 2000-2020. Note that i) the values for $\Delta H_{gl,1-2}$ for Ellsworth and Columbia refer to the period 1960-2000, and ii) the values for $\Delta H_{gl,3}$ are an average of the 2000-2005, 2005-2010, 2010-2015, and 2015-2020 changes. “ $H_{gl,E}$ ” and “ $H_{gl,M}$ ” are the median thicknesses of the glacier within the instability-adjacent glacier polygon from Farinotti et al. (2019) and Millan et al. (2022), respectively.

	Ellsworth	Portage	Barry	Yale	Columbia	Tyndall	Alsek	Grand Plateau
<u>$\Delta H_{gl,1}$ [m a^{-1}]</u>		<u>-2.7</u>	<u>1.25</u>	<u>-5.61</u>		<u>-3.29</u>	<u>-1.33</u>	<u>-1.97</u>
<u>$\Delta H_{gl,2}$ [m a^{-1}]</u>	-1.22	<u>-1.7</u>	<u>0.48</u>	<u>-5.42</u>	-5.2	<u>-9.55</u>	<u>-1.81</u>	<u>-3.3</u>
<u>$\Delta H_{gl,3}$ [m a^{-1}]</u>	<u>-2.51</u>	<u>-1.62</u>	<u>-9.65</u>	<u>-2.18</u>	<u>-14.1</u>	<u>0.56</u>	<u>-2.85</u>	<u>-5.85</u>
<u>$H_{gl,E}$ [m]</u>	<u>220</u>	<u>170</u>	<u>230</u>	<u>210</u>	<u>660</u>	<u>120</u>	<u>260</u>	<u>480</u>
<u>$H_{gl,M}$ [m]</u>	<u>250</u>	<u>200</u>	<u>280</u>	<u>260</u>	<u>400</u>	<u>240</u>	<u>280</u>	<u>260</u>

1010 **Appendix G:** Meteorological analyses

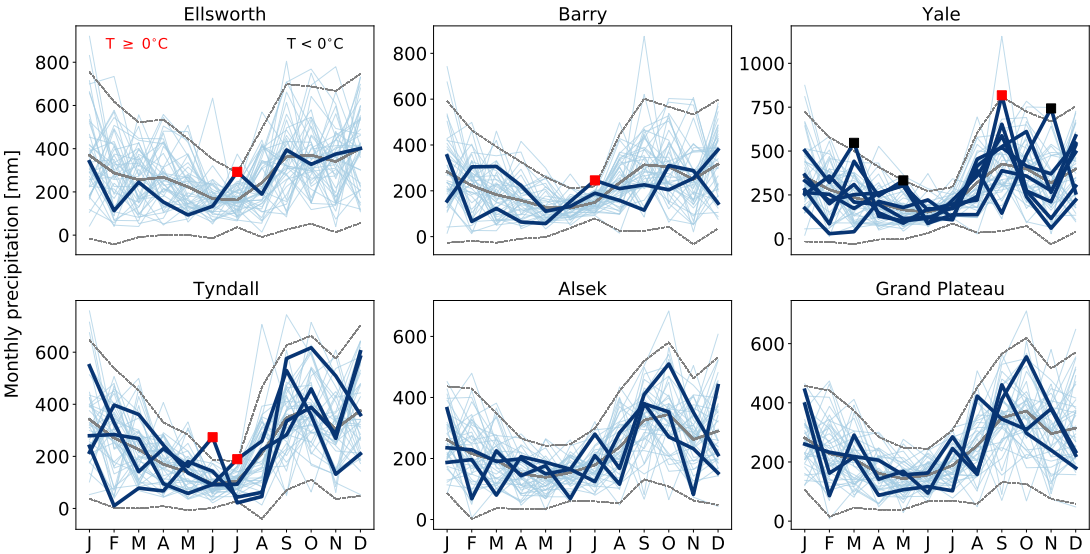


Figure G1. Average monthly precipitation at all sites which experienced a landslide acceleration during the study period. Thicker, darker blue lines correspond to the year or years during which the landslide accelerated, while light blue lines are all other years. The solid gray line corresponds to the mean monthly precipitation over the whole time period (1979-2022), and the gray dashed lines are two standard deviations above and below the mean. Red and black squares indicate temperatures above or below zero degrees, respectively, at instances where the monthly total during the activation period exceeded two standard deviations above the mean. Note the differing y-axes of the various subplots. All x-axes refer to the labels on the bottom row.

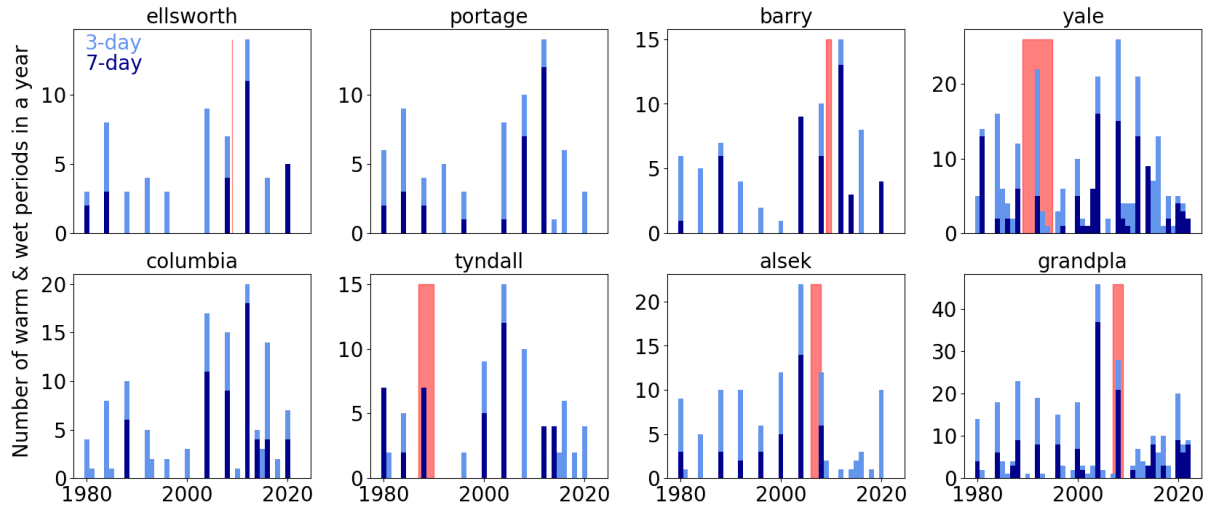


Figure G2. Occurrence of warm and wet periods in a year at the sites of interest. Light blue bars indicate the total number of days where the 3-day running precipitation total is greater than 3x the 90th precipitation quantile *and* the 3-day running temperature average was greater than 0°C. Dark blue bars are the total number of days where the 7-day running precipitation total is greater than 7x the 90th precipitation quantile *and* the 7-day running temperature average was greater than 0°C. Meteorological data comes from ERA5-Land (Muñoz-Sabater et al., 2021). In all panels, light red shading indicates the onset of landslide movement.

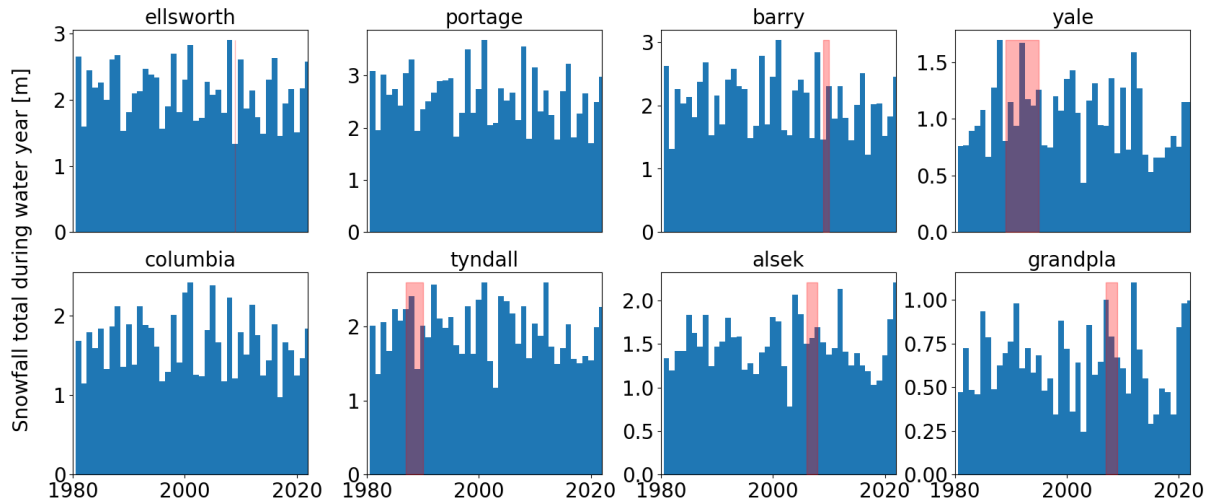


Figure G3. Snowfall total during the water year (Oct 1-Sep 30) at the sites of interest. Snowfall was calculated as the sum of all precipitation on days where the temperature was below 0°C (data from ERA5-Land; Muñoz-Sabater et al. (2021)). In all panels, light red shading indicates the onset of landslide movement.

Appendix H: Seismic analysis

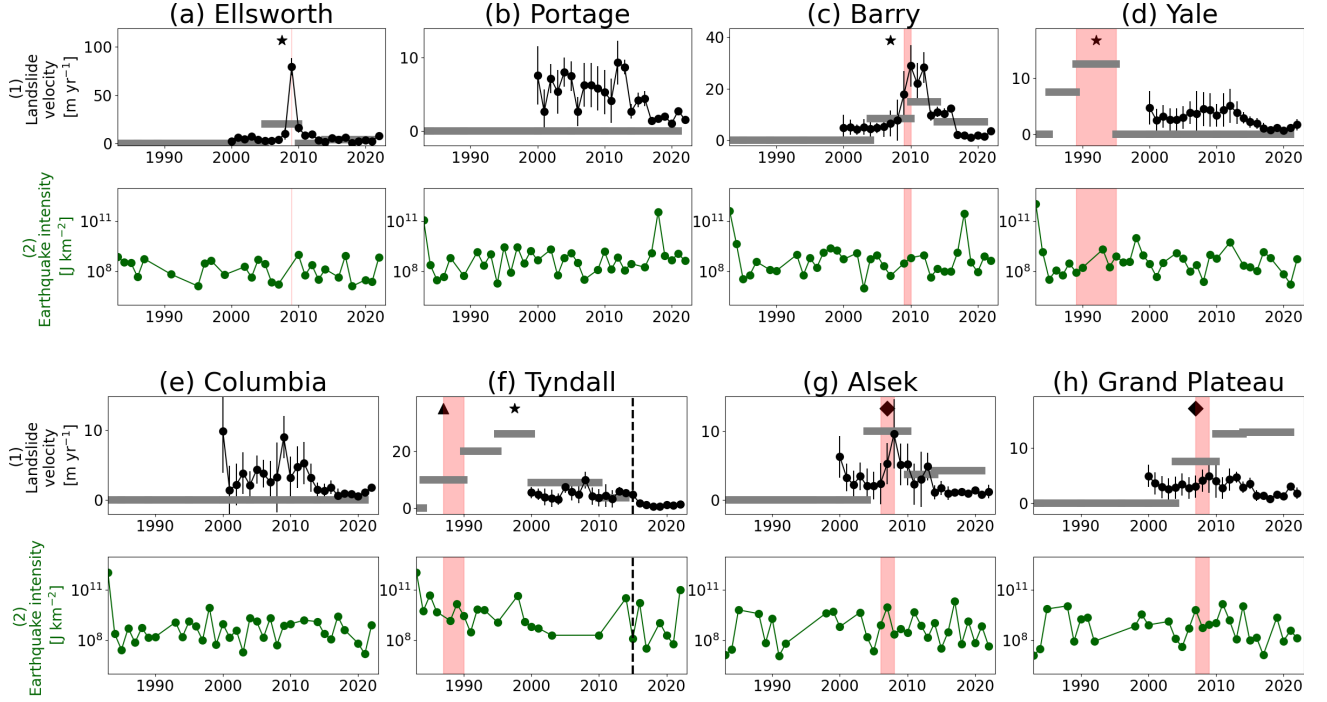


Figure H1. Landslide and earthquake intensity at the sites of interest. Row 1: Landslide velocities from ITS-LIVE (black circles, with vertical lines showing the uncertainty estimate from ITS-LIVE) and manual feature tracking (gray bars). Stars indicate onset of slope-wide deformation, triangles stand for crack opening, and diamonds mean both deformation and crack opening (in all cases the x-coordinate is the average over the time period in which the change was observed). Row 2: earthquake intensity at the instability (dark green), as calculated from U.S. Geological Survey (2023). In all panels, light red shading indicates the onset of landslide movement. At Tyndall, the black dashed line indicates a catastrophic failure. Note the differing scales on the y-axis for the individual sites.

Author contributions. MJ and BH conceptualized the study. JW completed the manual feature tracking analysis, mapped terminus locations, extracted ITS-LIVE velocities, and wrote the manuscript with the help of MJ and DF. BH provided landslide polygons and volumes, as well as helpful discussion about possible mechanisms. RH generated all co-registered DEMs. AM aided with the feature tracking and explanations of possible landslide mechanisms. DF supervised the overall work progress and helped in designing the figures. All co-authors read and provided feedback on the paper.

Competing interests. The authors declare that they have no conflict of interest.

Acknowledgements. We thank Maximillian Van Wyk de Vries and Amaury Dehecq for the helpful discussions about feature tracking, as well as Marit van Tiel for the useful input about glacier hydrology. We also thank Etienne Berthier and Amaury Dehecq for providing the 1960s and 1980s DEMs, respectively. Additionally, we thank Daniel Ben-Yehoshua for the interesting discussions about landslide-glacier interactions. BH acknowledges funding from the US National Science Foundation, award number 205210. RH acknowledges funding from the Swiss National Science Foundation, grant number 184634, as well as funding from NASA, award number 80NSSC22K1094. We would also like to thank Stuart Dunning, an anonymous reviewer, and the editor Andreas Günther for their helpful feedback which improved the manuscript.

- Agliardi, F., Scuderi, M. M., Fusi, N., and Collettini, C.: Slow-to-fast transition of giant creeping rockslides modulated by undrained loading in basal shear zones, *Nature Communications*, 11, <https://doi.org/10.1038/s41467-020-15093-3>, 2020.
- Alaska Seismic Hazards Safety Commission: Report to the Governor and State Legislature, https://seismic.alaska.gov/download/ashsc_meetings_minutes/ASHSC_2012_annual_report.pdf, 2012.
- 1030 Amundson, J., Truffer, M., Lüthi, M. P., Fahnstock, M., West, M., and Motyka, R. J.: Glacier, fjord, and seismic response to recent large calving events, Jakobshavn Isbræ, Greenland, *Geophysical Research Letters*, 35, doi:10.1029/2008GL035281, 2008.
- Ballantyne, C. K.: Paraglacial geomorphology, *Quaternary Science Reviews*, p. 83, 2002.
- Benn, D. I., Warren, C. R., and Mottram, R. H.: Calving processes and the dynamics of calving glaciers, *Earth Science Reviews*, 82, 143–179, <https://doi.org/10.1016/j.earscirev.2007.02.002>, 2007.
- 1035 Berthier, E., Schiefer, E., Clarke, G. K. C., Menounos, B., and Rémy, F.: Contribution of Alaskan Glaciers to Sea-Level Rise Derived from Satellite Imagery, *Nature Geoscience*, 3, 92–95, <https://doi.org/10.1038/ngeo737>, 2010.
- Blasio, F. D.: Introduction to the Physics of Landslides, chap. Friction, Cohesion, and Slope Stability, Springer, https://doi.org/10.1007/978-94-007-1122-8_2, 2011.
- Bovis, M. and Stewart, T.: Long-term deformation of a glacially undercut rock slope, southwest British Columbia, in: Eighth International Congress, International Association for Engineering Geology and the Environment, edited by Moore, D. and Hungr, O., A.A. Balkema Publishers, 1998.
- 1040 Brain, M. J., Moya, S., Kincey, M. E., Tunstall, N., Petley, D. N., and Sepúlveda, S. A.: Controls on Post-Seismic Landslide Behavior in Brittle Rocks, *Journal of Geophysical Research: Earth Surface*, 126, <https://doi.org/10.1029/2021JF006242>, 2021.
- Carrière, S. R., Jongmans, D., Chambon, G., Bièvre, G., Lanson, B., Bertello, L., Berti, M., Jaboyedoff, M., Malet, J.-P., and Chambers, J. E.: Rheological properties of clayey soils originating from flow-like landslides, *Landslides*, 15, 1615–1630, <https://doi.org/10.1007/s10346-018-0972-6>, 2018.
- 1045 Church, M. and Ryder, J. M.: Paraglacial Sedimentation: A Consideration of Fluvial Processes Conditioned by Glaciation, *GSA Bulletin*, 83, 3059–72, [https://doi.org/10.1130/0016-7606\(1972\)83\[3059:PSACOF\]2.0.CO;2](https://doi.org/10.1130/0016-7606(1972)83[3059:PSACOF]2.0.CO;2), 1972.
- Cody, E., Anderson, B. M., McColl, S. T., Fuller, I. C., and Purdie, H. L.: Paraglacial adjustment of sediment slopes during and immediately after glacial debuttreasing, *Geomorphology*, 371, 107411, <https://doi.org/10.1016/j.geomorph.2020.107411>, 2020.
- 1050 Cohen, S. C. and Freymueller, J. T.: Crustal Uplift in the South Central Alaska Subduction Zone: New Analysis and Interpretation of Tide Gauge Observations, *Journal of Geophysical Research: Solid Earth*, 106, 11 259–70, <https://doi.org/10.1029/2000JB900419>, 2001.
- Cuffey, K. M. and Paterson, W. S. B.: *The Physics of Glaciers*, Amsterdam Heidelberg: Butterworth-Heineman, 4 edn., 2010.
- Dahl-Jensen, T., Larsen, L. M., Pedersen, S. A. S., Pedersen, J., Jepsen, H. F., Pedersen, G., Nielsen, T., Pedersen, A. K., Platen-Hallermund, F. V., and Weng, W.: Landslide and Tsunami 21 November 2000 in Paatuut, West Greenland, *Natural Hazards*, 31, 277–87, <https://doi.org/10.1023/B:NHAZ.0000020264.70048.95>, 2004.
- 1055 Dai, C., Higman, B., Lynett, P. J., Jacquemart, M., Howat, I. M., Liljedahl, A. K., Dufresne, A., Freymueller, J. T., Geertsema, M., Ward Jones, M., and Haeussler, P. J.: Detection and Assessment of a Large and Potentially Tsunamigenic Periglacial Landslide in Barry Arm, Alaska, *Geophysical Research Letters*, 47, <https://doi.org/10.1029/2020GL089800>, 2020.

- Dehecq, A., Gardner, A. S., nad Scott McMichael, O. A., Hugonnet, R., Shean, D., and Marty, M.: Automated Processing of De-classified KH-9 Hexagon Satellite Images for Global Elevation Change Analysis Since the 1970s, *Frontiers in Earth Science*, 8, <https://www.frontiersin.org/articles/10.3389/feart.2020.566802>, 2020.
- Doi, I., Matsuura, S., Osawa, H., Shibasaki, T., and Tosa, S.: Effects of Coastal Erosion on Landslide Activity Revealed by Multi-sensor Observations, *Earth Surface Processes and Landforms*, 45, 2291–99, <https://doi.org/10.1002/esp.4880>, 2020.
- Earthquake Hazards Program: 20 Largest Earthquakes in the World Since 1900, united States Geological Survey, <https://www.usgs.gov/programs/earthquake-hazards/science/20-largest-earthquakes-world-1900>, 2019.
- Earthquake Hazards Program: Earthquake Magnitude, Energy Release, and Shaking Intensity, <https://www.usgs.gov/programs/earthquake-hazards/earthquake-magnitude-energy-release-and-shaking-intensity>, 2024.
- Epprecht, W.: A Major Calving Event of Jakobshavns Isbræ, West Greenland, on 9 August 1982, *Journal of Glaciology*, 33, 169–172, doi:10.3189/S0022143000008650, 1987.
- Falkner, K. K., Melling, H., Münchow, A. M., Box, J. E., Wohlleben, T., Johnson, H. L., Gudmandsen, P., Samelson, R., Copland, L., Steffen, K., Rignot, E., and Higgins, A. K.: Context for the Recent Massive Petermann Glacier Calving Event, *EOS, Transactions, AGU*, 92, 117–118, <https://doi.org/10.1029/2011EO140001>, 2011.
- Fan, X., Dufresne, A., Subramanian, S. S., Strom, A., Hermanns, R., Stefanelli, C. T., Hewitt, K., Yunus, A. P., Dunning, S., Capra, L., Geertsema, M., Miller, B., Casagli, N., Jansen, J. D., and Xu, Q.: The Formation and Impact of Landslide Dams – State of the Art, *Earth-Science Reviews*, 203, <https://doi.org/10.1016/j.earscirev.2020.103116>, 2020.
- Farinotti, D., Huss, M., Fürst, J. J., Landmann, J., Machguth, H., Maussion, F., and Pandit, A.: A consensus estimate for the ice thickness distribution of all glaciers on Earth, *Nature Geoscience*, 12, 168–173, <https://doi.org/10.1038/s41561-019-0300-3>, 2019.
- Federico, A., Popescu, M., Elia, G., Fidelibus, C., Internò, G., and Murianni, A.: Prediction of time to slope failure: a general framework, *Environmental Earth Sciences*, 66, 245–256, <https://doi.org/10.1007/s12665-011-1231-5>, 2011.
- Gardner, A. S., Moholdt, G., Scambos, T., Fahnestock, M., Ligtenberg, S., van den Broeke, M., and Nilsson, J.: Increased West Antarctic and unchanged East Antarctic ice discharge over the last 7 years, *The Cryosphere*, 12, 521–547, <https://doi.org/10.5194/tc-12-521-2018>, publisher: Copernicus GmbH, 2018.
- Gardner, A. S., Fahnestock, M. A., and Scambos, T. A.: ITS_LIVE Regional Glacier and Ice Sheet Surface Velocities: Version 2, data archived at National Snow and Ice Data Center; <https://doi.org/10.5067/6II6VW8LLWJ7>, 2023.
- Gischig, V., Preisig, G., and Eberhardt, E.: Numerical Investigation of Seismically Induced Rock Mass Fatigue as a Mechanism Contributing to the Progressive Failure of Deep-Seated Landslides, *Rock Mechanics and Rock Engineering*, 49, 2457–78, <https://doi.org/10.1007/s00603-015-0821-z>, 2016.
- Glueer, F., Loew, S., Manconi, A., and Aaron, J.: From Toppling to Sliding: Progressive Evolution of the Moosfluh Landslide, Switzerland, *Journal of Geophysical Research: Earth Surface*, 124, 2899–2919, <https://doi.org/10.1029/2019JF005019>, 2019.
- Glueer, F., Loew, S., and Manconi, A.: Paraglacial history and structure of the Moosfluh landslide (1850-2016), Switzerland, *Geomorphology*, 355, <https://doi.org/10.1016/j.geomorph.2019.02.021>, 2020.
- Google Earth Pro: Portage Glacier, Alaska, USA. 60°45′05.98″N, 148°48′39.26″W, eye alt 1.80km. U.S. Geological Survey and Landsat/-Copernicus., a.
- Google Earth Pro: Portage Glacier, Alaska, USA. 60°45′05.98″N, 148°48′39.26″W, eye alt 1.80km. Municipality of Anchorage., b.

- Grämiger, L. M., Moore, J. R., Gischig, V. S., Ivy-Ochs, S., and Loew, S.: Beyond Debuttressing: Mechanics of Paraglacial Rock Slope Damage during Repeat Glacial Cycles: PARAGLACIAL ROCK SLOPE MECHANICS, *Journal of Geophysical Research: Earth Surface*, 122, 1004–36, <https://doi.org/10.1002/2016JF003967>, 2017.
- Grämiger, L. M., Moore, J. R., Gischig, V. S., and Loew, S.: Thermomechanical Stresses Drive Damage of Alpine Valley Rock Walls During Repeat Glacial Cycles, *Journal of Geophysical Research: Earth Surface*, 123, 2620–46, <https://doi.org/10.1029/2018JF004626>, 2018.
- Grämiger, L. M., Moore, J. R., Gischig, V. S., Loew, S., Funk, M., and Limpach, P.: Hydromechanical Rock Slope Damage During Late Pleistocene and Holocene Glacial Cycles in an Alpine Valley, *Journal of Geophysical Research: Earth Surface*, 125, <https://doi.org/10.1029/2019JF005494>, 2020.
- Guzzetti, F., Ardizzone, F., Cardinali, M., Rossi, M., and Valigi, D.: Landslide volumes and landslide mobilization rates in Umbria, central Italy, *Earth and Planetary Science Letters*, 279, 222–229, <https://doi.org/10.1016/j.epsl.2009.01.005>, 2009.
- Handwerger, A. L., Fielding, E. J., Huang, M., Bennett, G. L., Liang, C., and Schulz, W. H.: Widespread Initiation, Reactivation, and Acceleration of Landslides in the Northern California Coast Ranges Due to Extreme Rainfall, *Journal of Geophysical Research: Earth Surface*, 124, 1782–97, <https://doi.org/10.1029/2019JF005035>, 2019a.
- Handwerger, A. L., Huang, M.-H., Fielding, E. J., Booth, A. M., and Bürgmann, R.: A shift from drought to extreme rainfall drives a stable landslide to catastrophic failure, *Scientific Reports*, 9, <https://doi.org/10.1038/s41598-018-38300-0>, 2019b.
- Handwerger, A. L., Fielding, E. J., Sangha, S. S., and Bekaert, D. P. S.: Landslide Sensitivity and Response to Precipitation Changes in Wet and Dry Climates, *Geophysical Research Letters*, 49, <https://doi.org/10.1029/2022GL099499>, 2022.
- Hanson, B. and Hooke, R. L.: Glacier Calving: A Numerical Model of Forces in the Calving-Speed/Water-Depth Relation, *Journal of Glaciology*, 46, 188–96, <https://doi.org/10.3189/172756500781832792>, 2000.
- Hendron, A. and Patton, F.: The Vaiont Slide — A Geotechnical Analysis Based on New Geologic Observations of the Failure Surface, *Engineering Geology*, 24, 475–91, [https://doi.org/10.1016/0013-7952\(87\)90080-9](https://doi.org/10.1016/0013-7952(87)90080-9), 1987.
- Hermanns, R. L., Schleier, M., Böhme, M., Blikra, L. H., Gosse, J., Ivy-Ochs, S., and Hilger, P.: Rock-Avalanche Activity in W and S Norway Peaks After the Retreat of the Scandinavian Ice Sheet, in: *Advancing Culture of Living with Landslides*, edited by Mikoš, M., Vilímek, V., Yin, Y., and Sassa, K., pp. 331–38, Springer International Publishing, 2017.
- Hersbach, H., Muñoz Sabater, J., Nicolas, Rozum, I., Simmons, Vamborg, F., Bell, B., Berrisford, P., Biavati, G., Buontempo, C., Horányi, A., Peubey, C., Radu, R., Schepers, D., Soci, C., Dee, D., and Thépaut, J.-N.: Essential climate variables for assessment of climate variability from 1979 to present, copernicus Climate Change Service (C3S) Data Store (CDS). (Accessed on 11-11-2022), 2018.
- Higman, B.: Alaska inventory of landslides and slope instabilities, accessed April 12, 2022, 2022.
- Higman, B., Shugar, D. H., Stark, C. P., Ekström, G., Koppes, M. N., Lynett, P., Dufresne, A., Haeussler, P. J., Geertsema, M., Gulick, S., Mattox, A., Venditti, J. G., Walton, M. A. L., McCall, N., Mckittrick, E., MacInnes, B., Bilderback, E. L., Tang, H., Willis, M. J., Richmond, B., Reece, R. S., Larsen, C., Olson, B., Capra, J., Ayca, A., Bloom, C., Williams, H., Bonno, D., Weiss, R., Keen, A., Skanavis, V., and Loso, M.: The 2015 landslide and tsunami in Taan Fiord, Alaska, *Scientific Reports*, 8, 12993, <https://doi.org/10.1038/s41598-018-30475-w>, 2018.
- Higman, B., Lahusen, S., Belair, G., Staley, D., and Jacquemart, M.: Inventory of Large Slope Instabilities, Prince William Sound, Alaska: U.S. Geological Survey data release, <https://doi.org/10.5066/P9XGMHHP>, 2023.
- Hugentobler, M., Loew, S., Aaron, J., Roques, C., and Oestreicher, N.: Borehole Monitoring of Thermo-Hydro-Mechanical Rock Slope Processes Adjacent to an Actively Retreating Glacier, *Geomorphology*, 362, <https://doi.org/10.1016/j.geomorph.2020.107190>, 2020.

- Hugentobler, M., Aaron, J., Loew, S., and Roques, C.: Hydro-Mechanical Interactions of a Rock Slope With a Retreating Temperate Valley Glacier, *Journal of Geophysical Research: Earth Surface*, 127, <https://doi.org/10.1029/2021JF006484>, 2022.
- 1135 Hugonnet, R., McNabb, R., Berthier, E., Menounos, B., Nuth, C., Girod, L., Farinotti, D., Huss, M., Dussaillant, I., Brun, F., and Kääb, A.: Accelerated global glacier mass loss in the early twenty-first century, *Nature*, 592, 726–731, <https://doi.org/10.1038/s41586-021-03436-z>, 2021.
- Hussain, M. and Mahmud, I.: pyMannKendall: a python package for non parametric Mann Kendall family of trend tests., *Journal of Open Source Software*, 4, 1556, <https://doi.org/10.21105/joss.01556>, 2019.
- 1140 Immerzeel, W. W., Lutz, A. F., Andrade, M., Bahl, A., Biemans, H., Bolch, T., Hyde, S., Davies, B., Elmore, A. C., Emmer, A., Feng, M., Fernández, A., Haritashya, U., Kargel, J. S., Koppes, M., Kraaijenbrink, P. D. A., Kulkarni, A. V., Mayewski, P. A., Nepal, S., Pacheco, P., Painter, T. H., Pellicciotti, F., Rajaram, H., Rupper, S., Sinisalo, A., Shrestha, A. B., Viviroli, D., Wada, Y., Xiao, C., Yao, T., and Baillie, J. E. M.: Importance and Vulnerability of the World’s Water Towers, *Nature*, 577, 364–69, <https://doi.org/10.1038/s41586-019-1822-y>, 2020.
- 1145 IPCC: Summary for Policymakers, in: IPCC Special Report on the Ocean and Cryosphere in a Changing Climate, edited by Pörtner, H. O., Roberts, D., Masson-Delmotte, V., Zhai, V., Tignor, M., Poloczanska, E., Mintenbeck, K., Alegría, A., Nicolai, M., Okem, A., Petzold, J., Rama, B., and Weyer, N., pp. 3–35, Cambridge University Press, Cambridge, UK and New York, NY, USA, <https://doi.org/10.1017/9781009157964.001>, 2019.
- IPCC: in: Climate Change 2022: Impacts, Adaptation, and Vulnerability. Contribution of Working Group II to the Sixth Assessment Report of the Intergovernmental Panel on Climate Change, edited by Pörtner, H. O., Roberts, D., Tignor, M., Poloczanska, E., Mintenbeck, K., Alegría, A., Craig, M., Langsdorf, S., Löschke, S., Möller, V., Okem, A., and Rama, B., p. 3056, Cambridge University Press, Cambridge, UK and New York, NY, USA, doi:10.1017/9781009325844, 2022.
- 1150 Iverson, R. M.: Landslide Triggering by Rain Infiltration, *Water Resources Research*, 36, 1897–1910, <https://doi.org/10.1029/2000WR900090>, 2000.
- 1155 Iverson, R. M., Reid, M. E., Iverson, N. R., LaHusen, R. G., Logan, M., Mann, J. E., and Brien, D. L.: Acute Sensitivity of Landslide Rates to Initial Soil Porosity, *Science*, 290, 513–516, <https://doi.org/10.1126/science.290.5491.513>, 2000.
- Jaboyedoff, M., Carrea, D., Derron, M.-H., Oppikofer, T., Penna, I. M., and Rudaz, B.: A Review of Methods Used to Estimate Initial Landslide Failure Surface Depths and Volumes, *Engineering Geology*, 267, <https://doi.org/10.1016/j.enggeo.2020.105478>, 2020.
- Jansson, P., Hock, R., and Schneider, T.: The Concept of Glacier Storage: A Review, *Journal of Hydrology*, 282, 116–29, [https://doi.org/10.1016/S0022-1694\(03\)00258-0](https://doi.org/10.1016/S0022-1694(03)00258-0), 2003.
- 1160 Jeffries, S.: Columbia Glacier GPS (CBIA), earthScope Consortium, GPS Continuous Station Data Set, <https://www.unavco.org/instrumentation/networks/status/nota/overview/CBIA>, accessed 9 August 2024, time-windowed subset 2023-07-29 through 2024-07-29, 2023.
- Kanamori, H.: The Energy Release in Great Earthquakes, *Journal of Geophysical Research*, 82, 2981–87, <https://doi.org/10.1029/JB082i020p02981>, 1977.
- 1165 Keefer, D. K.: Landslides caused by earthquakes, *GSA Bulletin*, 4, 406–421, 1984.
- Kim, J., Coe, J. A., Lu, Z., Avdievitch, N. N., and Hults, C. P.: Spaceborne InSAR Mapping of Landslides and Subsidence in Rapidly Deglaciating Terrain, Glacier Bay National Park and Preserve and Vicinity, Alaska and British Columbia, *Remote Sensing of Environment*, 281, 113 231, <https://doi.org/10.1016/j.rse.2022.113231>, 2022.

- 1170 Kohler, M. and Puzrin, A.: Mechanics of coseismic and postseismic acceleration of active landslides, *Communications Earth Environment*, 4, <https://doi.org/10.1038/s43247-023-00797-3>, 2023.
- Kos, A., Amann, F., Strozzi, T., Delaloye, R., Ruetten, J., and Springman, S.: Contemporary glacier retreat triggers a rapid landslide response, Great Aletsch Glacier, Switzerland, *Geophysical Research Letters*, 43, <https://doi.org/10.1002/2016GL071708>, 2016.
- Kuhn, D., Hermanns, R. L., Torizin, J., Fuchs, J. M., Schüßler, N., Eilertsen, R. S., Redfield, T. F., Balzer, D., and Böhme, M.: Litho-
1175 Structural Control on Rock Slope Failures at Garmaksla, Billefjorden Coastline, Svalbard, *Quarterly Journal of Engineering Geology and Hydrogeology*, 56, <https://doi.org/10.1144/qjagh2022-069>, 2023.
- Lacroix, P. and Amitrano, D.: Long-term dynamics of rockslides and damage propagation inferred from mechanical modeling, *Journal of Geophysical Research*, 118, 2292–2307, doi:10.1002/2013JF002766, 2013.
- Lacroix, P., Perfettini, H., Taipei, E., and Guillier, B.: Coseismic and postseismic motion of a landslide: Observations, modeling, and analogy
1180 with tectonic faults, *Geophysical Research Letters*, 41, 6676–6680, <https://doi.org/10.1002/2014GL061170>, 2014.
- Lacroix, P., Handwerger, A. L., and Bièvre, G.: Life and Death of Slow-Moving Landslides, *Nature Reviews Earth & Environment*, 1, 404–19, <https://doi.org/10.1038/s43017-020-0072-8>, 2020.
- Lacroix, P., Belart, J. M. C., Berthier, E., Sæmundsson, P., and Jónsdóttir, K.: Mechanisms of Landslide Destabilization Induced by Glacier-Retreat on Tungnakvíslarjökull Area, Iceland, *Geophysical Research Letters*, 49, <https://doi.org/10.1029/2022GL098302>, 2022.
- 1185 Larsen, C., Motyka, R., Freymueller, J., Echelmeyer, K., and Ivins, E.: Rapid Viscoelastic Uplift in Southeast Alaska Caused by Post-Little Ice Age Glacial Retreat, *Earth and Planetary Science Letters*, 237, 548–60, <https://doi.org/10.1016/j.epsl.2005.06.032>, 2005.
- Le Roux, O., Schwartz, S., Gamond, J. F., Jongmans, D., Bourles, D., Braucher, R., Mahaney, W., Carcaillet, J., and Leanni, L.: CRE dating on the head scarp of a major landslide (Séchilienne, French Alps), age constraints on Holocene kinematics, *Earth and Planetary Science Letters*, 280, 236–245, <https://doi.org/10.1016/j.epsl.2009.01.034>, 2009.
- 1190 Lemaire, E., Dufresne, A., Hamdi, P., Hignman, B., Wolken, G. J., and Amann, F.: Back-Analysis of the Paraglacial Slope Failure at Grewingk Glacier and Lake, Alaska, *Landslides*, <https://doi.org/10.1007/s10346-023-02177-6>, 2023a.
- Lemaire, E., Dufresne, A., Hamdi, P., Hignman, B., Jacquemart, M., Walden, J., and Amann, F.: Analysis of the unstable slope above Portage Glacier (Alaska) through conventional and remote sensing approaches, 6th World Landslide Forum, Florence, Italy, THEME 2: REMOTE SENSING, MONITORING AND EARLY WARNING, 2023b.
- 1195 Loso, M. G., Larsen, C. F., Tober, B. S., Christoffersen, M., Fahnestock, M., Holt, J. W., and Truffer, M.: Quo Vadis, Alsek? Climate-Driven Glacier Retreat May Change the Course of a Major River Outlet in Southern Alaska, *Geomorphology*, 384, 107 701, <https://doi.org/10.1016/j.geomorph.2021.107701>, 2021.
- Luckman, A., Benn, D., Cottier, F., Bevan, S., Nilsen, F., and Inall, M.: Calving rates at tidewater glaciers vary strongly with ocean temperature, *Nature Communications*, 6, <https://doi.org/10.1038/ncomms9566>, 2015.
- 1200 Mainsant, G., Larose, E., Brönnimann, C., Jongmans, D., Michoud, C., and Jaboyedoff, M.: Ambient seismic noise monitoring of a clay landslide: Toward failure prediction, *Journal of Geophysical Research*, 117, doi:10.1029/2011JF002159, 2012.
- Manconi, A.: How Phase Aliasing Limits Systematic Space-Borne DInSAR Monitoring and Failure Forecast of Alpine Landslides, *Engineering Geology*, 287, 106 094, <https://doi.org/10.1016/j.enggeo.2021.106094>, 2021.
- McColl, S. T.: Landslide Causes and Triggers, in: *Landslide Hazards, Risks, and Disasters*, pp. 17–42, Elsevier, <https://doi.org/10.1016/B978-0-12-396452-6.00002-1>, 2015.
- 1205

- McColl, S. T. and Davies, T. R. H.: Large ice-contact slope movements: glacial buttressing, deformation and erosion: Slope movement; glacier deformation; erosion and entrainment, *Earth Surface Processes and Landforms*, 38, 1102–1115, <https://doi.org/10.1002/esp.3346>, 2013.
- McColl, S. T., Davies, T. R. H., and McSaveney, M. J.: Glacier retreat and rock-slope stability: debunking debuttressing, geologically active : delegate papers 11th Congress of the International Association for Engineering Geology and the Environment, Auckland, Aotearoa, 5-10 September 2010. Auckland, New Zealand; pp. 467-474., 2010.
- McNabb, R. W., Hock, R., and Huss, M.: Variations in Alaska tidewater glacier frontal ablation, 1985–2013, *Journal of Geophysical Research: Earth Surface*, 120, 120–136, <https://doi.org/10.1002/2014JF003276>, 2015.
- Millan, R., Mouginot, J., Rabatel, A., and Morlighem, M.: Ice velocity and thickness of the world’s glaciers, *Nature Geoscience*, 15, 124–129, <https://doi.org/10.1038/s41561-021-00885-z>, number: 2 Publisher: Nature Publishing Group, 2022.
- Miller, D. J.: The Alaska earthquake of July 10, 1958: Giant wave in Lituya Bay, *Bulletin of the Seismological Society of America*, 50, 253–266, <https://doi.org/10.1785/BSSA0500020253>, 1960.
- Muñoz-Sabater, J., Dutra, E., Agustí-Panareda, A., Albergel, C., Arduini, G., Balsamo, G., Boussetta, S., Choulga, M., Harrigan, S., Hersbach, H., Martens, B., Miralles, D. G., Piles, M., Rodríguez-Fernández, N. J., Zsoter, E., Buontempo, C., and Thépaut, J.-N.: ERA5-Land: A State-of-the-Art Global Reanalysis Dataset for Land Applications, *Earth System Science Data*, 13, 4349–83, <https://doi.org/10.5194/essd-13-4349-2021>, 2021.
- Mériaux, A., Sieh, K., Finkel, R. C., Rubin, C. M., Taylor, M. H., Meltzner, A. J., and Ryerson, F. J.: Kinematic Behavior of Southern Alaska Constrained by Westward Decreasing Postglacial Slip Rates on the Denali Fault, Alaska, *Journal of Geophysical Research: Solid Earth*, 114, <https://doi.org/10.1029/2007JB005053>, 2009.
- Nuth, C. and Kääb, A.: Co-Registration and Bias Corrections of Satellite Elevation Data Sets for Quantifying Glacier Thickness Change, *The Cryosphere*, 5, 271–90, <https://doi.org/10.5194/tc-5-271-2011>, 2011.
- Obu, J., Westermann, S., Kääb, A., and Bartsch, A.: Ground Temperature Map, 2000-2016, Northern Hemisphere Permafrost, alfred Wegener Institute, Helmholtz Centre for Polar and Marine Research, Bremerhaven, PANGAEA, <https://doi.org/10.1594/PANGAEA.888600>, 2018.
- Oestreicher, N., Loew, S., Roques, C., Aaron, J., Gualandi, A., Longuevergne, L., Limpach, P., and Hugentobler, M.: Controls on Spatial and Temporal Patterns of Slope Deformation in an Alpine Valley, *Journal of Geophysical Research: Earth Surface*, 126, <https://doi.org/10.1029/2021JF006353>, 2021.
- Okal, E. A.: Seismic Parameters Controlling Far-Field Tsunami Amplitudes: A Review, *Natural Hazards*, 1, 67–96, <https://doi.org/10.1007/BF00168222>, 1988.
- O’Neel, S., Pfeffer, W. T., Krimmel, R., and Meier, M.: Evolving force balance at Columbia Glacier, Alaska, during its rapid retreat, *Journal of Geophysical Research*, 110, <https://doi.org/10.1029/2005JF000292>, 2005.
- Paronuzzi, P., Rigo, E., and Bolla, A.: Influence of Filling–Drawdown Cycles of the Vajont Reservoir on Mt. Toc Slope Stability, *Geomorphology*, 191, 75–93, <https://doi.org/10.1016/j.geomorph.2013.03.004>, 2013.
- Payo, A., Hall, J. W., French, J., Sutherland, J., Maanen, B. V., Nicholls, R. J., and Reeve, D. E.: Causal Loop Analysis of Coastal Geomorphological Systems, *Geomorphology*, 256, 36–48, <https://doi.org/10.1016/j.geomorph.2015.07.048>, 2016.
- Porter, C., Morin, P., Howat, I., Noh, M.-J., Bates, B., Peterman, K., Keesey, S., Schlenk, M., Gardiner, J., Tomko, K., Willis, M., Kelleher, C., Cloutier, M., Husby, E., Foga, S., Nakamura, H., Platson, M., Wethington, Michael, J., Williamson, C., Bauer, G., Enos, J., Arnold, G., Kramer, W., Becker, P., Doshi, A., D’Souza, C., Cummens, P., Laurier, F., and Bojesen, M.: ArcticDEM, Version 3, <https://doi.org/10.7910/DVN/OHHUKH>, 2018.

- Ravier, E. and Buoncristiani, J.-F.: Glaciohydrogeology, in: *Past Glacial Environments*, pp. 431–66, Elsevier, <https://doi.org/10.1016/B978-0-08-100524-8.00013-0>, 2018.
- RGI Consortium: Randolph Glacier Inventory - A Dataset of Global Glacier Outlines, Version 6, boulder, Colorado USA. NSIDC: National Snow and Ice Data Center. doi: <https://doi.org/10.7265/4m1f-gd79>, 2017.
- Rounce, D. R., Hock, R., Maussion, F., Hugonnet, R., Kochtitzky, W., Huss, M., Berthier, E., Brinkerhoff, D., Compagno, L., Copland, L., Farinotti, D., Menounos, B., and McNabb, R. W.: Global Glacier Change in the 21st Century: Every Increase in Temperature Matters, *Science*, 379, 78–83, <https://doi.org/10.1126/science.abo1324>, 2023.
- Schaefer, L., Coe, J. A., Jones, K. W., Collins, B. D., Staley, D. M., West, M., Karasozen, E., Miles, C., Wolken, G., Daanen, R., and Baxstrom, K.: Kinematic Evolution of a Large Paraglacial Landslide in the Barry Arm Fjord of Alaska, *Journal of Geophysical Research: Earth Surface*, 128, <https://doi.org/10.1029/2023JF007119>, 2023.
- Schaefer, L., Kim, J., Staley, D., Lu, Z., and Barnhart, K.: Satellite interferometry landslide detection and preliminary tsunamigenic plausibility assessment in Prince William Sound, southcentral Alaska, Tech. rep., U.S. Geological Survey Open-File Report 2023–1099, <https://doi.org/10.3133/ofr20231099>, 2024.
- Selley, R. C.: ROCKS AND THEIR CLASSIFICATION, in: *Encyclopedia of Geology*, edited by Selley, R. C., Cocks, L. R. M., and Plimer, I. R., p. 452–55, Oxford: Elsevier, <https://doi.org/10.1016/B0-12-369396-9/00288-4>, 2005.
- Sharma, S., Talchabhadel, R., Nepal, S., Ghimire, G. R., Rakhali, B., Panthi, J., Adhikari, B. R., Pradhanang, S. M., Maskey, S., and Kumar, S.: Increasing Risk of Cascading Hazards in the Central Himalayas, *Natural Hazards*, 119, 1117–26, <https://doi.org/10.1007/s11069-022-05462-0>, 2023.
- Shugar, D.H. et al.: A massive rock and ice avalanche caused the 2021 disaster at Chamoli, Indian Himalaya, *Science*, 373, 300–306, doi:10.1126/science.abh4455, 2021.
- Shulski, M. and Wendler, G.: *The Climate of Alaska*, University of Alaska Press, <https://books.google.ch/books?id=aUDWK8zDr50C>, 2007.
- Song, C., Yu, C., Li, Z., Utili, S., Frattini, P., Crosta, G., and Peng, J.: Triggering and Recovery of Earthquake Accelerated Landslides in Central Italy Revealed by Satellite Radar Observations, *Nature Communications*, 13, 7278, <https://doi.org/10.1038/s41467-022-35035-5>, 2022.
- Stead, D. and Wolter, A.: A critical review of rock slope failure mechanisms: The importance of structural geology, *Journal of Structural Geology*, 74, 1–23, <https://doi.org/10.1016/j.jsg.2015.02.002>, 2015.
- Storni, E., Hugentobler, M., Manconi, A., and Loew, S.: Monitoring and analysis of active rockslide-glacier interactions (Moosfluh, Switzerland), *Geomorphology*, 371, 107414, <https://doi.org/10.1016/j.geomorph.2020.107414>, 2020.
- Strzelecki, M. C. and Jaskólski, M. W.: Arctic tsunamis threaten coastal landscapes and communities – survey of Karrat Isfjord 2017 tsunami effects in Nuugaatsiaq, western Greenland, *Natural Hazards Earth System Science*, 20, 2521–2534, <https://doi.org/10.5194/nhess-20-2521-2020>, 2020.
- Svennevig, K. et al.: A rockslide-generated tsunami in a Greenland fjord rang Earth for 9 days, *Science*, 385, 1196–1205, doi:10.1126/science.adm9247, 2024.
- U.S. Geological Survey: Earthquakes, <https://earthquake.usgs.gov/earthquakes/map/>, 2023.
- U.S. Geological Survey and Alaska Department of Natural Resources: Quaternary Fault and Fold Database of the United States, <https://www.usgs.gov/programs/earthquake-hazards/faults>, 2024.
- Van Wyk de Vries, M., Wickert, A. D., MacGregor, K. R., Rada, C., and Willis, M. J.: Atypical landslide induces speedup, advance, and long-term slowdown of a tidewater glacier, *Geology*, <https://doi.org/10.1130/G49854.1>, 2022.

- Voight, B.: A method for prediction of volcanic eruptions, *Nature*, 332, <https://doi.org/10.1038/332125a0>, 1988.
- Wang, F., Zhang, Y., Huo, Z., Peng, X., Araiba, K., and Wang, G.: Movement of the Shuping landslide in the first four years after the initial impoundment of the Three Gorges Dam Reservoir, China, *Landslides*, 5, 321–329, <https://doi.org/10.1007/s10346-008-0128-1>, 2008.
- 1285 Wang, X., Clague, J. J., Crosta, G. B., Sun, J., Stead, D., Qi, S., and Zhang, L.: Relationship between the spatial distribution of landslides and rock mass strength, and implications for the driving mechanism of landslides in tectonically active mountain ranges, *Engineering Geology*, 292, <https://doi.org/10.1016/j.enggeo.2021.106281>, 2021.
- Warren, C., Benn, D., Winchester, V., and Harrison, S.: Buoyancy-driven lacustrine calving, Glaciar Nef, Chilean Patagonia, *Journal of Glaciology*, 47, 135–146, doi:10.3189/172756501781832403, 2001.
- 1290 Weertman, J.: Stability of the Junction of an Ice Sheet and an Ice Shelf, *Journal of Glaciology*, 13, 3–11, <https://doi.org/10.3189/S0022143000023327>, 1974.
- Wiles, G. C. and Calkin, P. E.: Reconstruction of a Debris-Slide-Initiated Flood in the Southern Kenai Mountains, Alaska, *Geomorphology*, 5, 535–46, [https://doi.org/10.1016/0169-555X\(92\)90024-I](https://doi.org/10.1016/0169-555X(92)90024-I), 1992.
- Wilson, F., Hults, C., Mull, C., and Karl, S.: Geologic map of Alaska: U.S. Geological Survey Scientific Investigations Map SIM-3340, 1295 <https://doi.org/10.3133/sim3340>, 2015.
- Windnagel, A., Hock, R., Maussion, F., Paul, F., Rastner, P., Raup, B., and Zemp, M.: Which glaciers are the largest in the world?, *Journal of Glaciology*, 69, 301–310, doi:10.1017/jog.2022.61, 2023.
- xDEM contributors: xDEM, Zenodo, <https://doi.org/10.5281/zenodo.4809697>, 2024.